# Hardness tests on irradiated pressure vessel steel

by

David James Harvey

A Thesis Submitted to the
Graduate Faculty in Partial Fulfillment of the
Requirements for the Degree of
MASTER OF SCIENCE

Major: Nuclear Engineering

Approved:



Iowa State University
Ames, Iowa

1980

TABLE OF CONTENTS

# INTRODUCTION

The general problem of radiation damage covers a broad spectrum of topics (swelling, embrittlement, etc.) and materials (fuel, fuel cladding, pressure vessels, etc.). The subject under discussion has been narrowed to radiation effects on steels for light-water-cooled reactor pressure vessels which will henceforth be referred to as RPV steels. In particular, the paper will cover radiation effects on the mechanical properties of RPV steels and the subsequent recovery of those properties upon annealing.

When considering pressure vessels, the main area of concern is the reactor beltline material, i.e., the material exposed to the highest neutron flux from the reactor core. This region is subject to an appreciable neutron flux of approximately $10^{11}$ neutrons per $cm^2$ per second with an energy greater than 1 MeV.

The steels used to construct the RPV are generally called mild or ferritic steels. The metal has a low carbon content, although not as low as in a stainless steel, and a body-centered cubic, bcc, crystal structure.

The two steels most commonly used in the construction of an RPV are ASTM A302 Grade B and ASTM A533 Grade B. The specifications for the composition of the steels are listed in Table 1. Table 2 lists the required mechanical properties.

Table 1. Compositions of reactor pressure vessel steels[a]

| Steel | C | Mn | P | S | Si | Mo | Ni |
|---|---|---|---|---|---|---|---|
| A302 B[b] | 0.20 max | 1.15-1.50 | 0.035 max | 0.040 max | 0.15-0.30 | 0.45-0.60 | --- |
| A533 B[c] | 0.25 max | 1.15-1.50 | 0.035 max | 0.040 max | 0.15-0.30 | 0.45-0.60 | 0.40-0.70 |

[a]All compositions are listed in weight percent with any balance being composed of iron.

[b]Values for A302 B are from reference 1.

[c]Values for A533 B are from reference 2.

Table 2. Tensile strength and yield strength for reactor pressure vessel steels

| Steel | Tensile Strength (ksi) | Yield Strength Minimum (ksi) |
|---|---|---|
| A302 B[a] | 80.0 - 100.0 | 50.0 |
| A533 B[b] | 80.0 - 100.0 | 50.0 |

[a]Values for A302 B are from reference 1.

[b]Values for A533 B are from reference 2.

## RADIATION EFFECTS ON THE MECHANICAL PROPERTIES OF METALS

When considering radiation effects on metals the main concern is neutron irradiation. In a reactor environment it is the neutron flux which causes all but a negligible fraction of the radiation damage, at least when considering the pressure vessel. Fission fragments have a considerable effect in the fuel but are not of concern with respect to radiation damage elsewhere because of their limited range.

When a neutron, with sufficient kinetic energy, impinges upon a metal it can cause damage by imparting some of that energy to a metal atom, causing that atom to be displaced from its lattice site. This displaced atom is called a primary knock-on atom, PKA, and it can, in turn, cause further displacements.

When an atom is displaced from its lattice site, two point defects are created; a vacancy and an interstitial. Collections of the point defects on a microscopic scale have macroscopic effects on mechanical properties.

### Radiation Hardening

The method by which the PKA and its associated defects can have an effect on the mechanical properties of metals was suggested by Seeger (3) in his zone theory of radiation hardening. Near the end of the path of the PKA there is a region of approximately spheroidal shape in which a considerable fraction, some 20 to 30%, of the atoms have been displaced. This region is variously called a displacement spike or a depleted zone. It is also noted that although some displaced atoms may be captured by

vacant sites within the same spike, there will remain zones with smaller density than the matrix.

A note should be made that although Seeger studied copper, which has a face-centered cubic, fcc, crystal structure, his work is also applicable to bcc metals.

For the zone theory of radiation hardening to be correct it must account for many experimental observations, including: (a) The critical shear stress, $\tau_o$, is found to be strongly dependent upon the temperature of deformation after irradiation, (b) The increase of $\tau_o$ is virtually independent of the temperature of irradiation, provided the irradiation takes place below the recovery temperature, $T_R$, (c) The radiation hardening of copper is unaffected by annealing below $T_R$, (d) The softening at $T_R$ occurs with an activation energy approximately equal to that of self-diffusion (3), (e) The softening is not accompanied by recrystallization.

The Seeger theory can in fact account for all of these observations. For (a) it explains the observed temperature dependence of $\tau_o$ since the cutting by dislocations through a forest of obstacles is both stress- and thermally-activated. The mechanism for zone formation, i.e., a depleted zone of reduced density formed by a PKA, is virtually temperature independent, as required in (b). The elimination of the hardening zones through annealing is possible only at temperatures where appreciable self-diffusion is possible, which satisfies (c). For (d) the theory predicts that the activation energy for softening should be approximately equal to, but slightly less than, that for self-diffusion.

Finally, (e) is satisfied because the zones can be eliminated by the migration of individual atoms (or whole zones) without the need for recrystallization. Another comment about observation (c) is also of importance. Observation (c), at least in the case for copper, shows that the main contribution to the radiation hardening by neutrons is not caused by isolated point defects, since, from annealing studies showing the recovery of electrical resistivity, it is known that the majority of point defects anneal out at temperatures below $T_R$.

The neutron irradiation induced hardening will then be taken to be caused by these depleted zones, after Seeger. A final note on the zone theory is it predicts that, in the absence of saturation effects, $\tau_o$ should be proportional to the square root of the fluence, $\Phi$. This idea will be covered in more detail later.

The zones that are created can cause two types of hardening; lattice and source hardening (4,5). The nucleation of slip, source hardening, and/or the propagation of slip, lattice hardening, is made more difficult. The Hall-Petch equation (6) provides a functional format by which the two processes can be sorted out

$$\sigma_y = \sigma_i + k_y d^{-1/2}$$

where $\sigma_y$ is the yield stress, $\sigma_i$ is the friction stress opposing dislocation motion, $k_y$ is a measure of the stress required to unpin the dislocations from barriers, and d is the grain diameter.

In the formation of these zones there is observed to be a saturation effect. Makin and Minter (5) take the saturation effect into account.

Simply stated, the saturation effect is an explanation for the observation that at high neutron doses the hardening rate decreases.

The theory for the cutting of an obstacle by a dislocation line suggests that $\sigma_i$ should be proportional to $N_z^{1/2}$, where $N_z$ is the obstacle density. $N_z$ is initially expected to be proportional to $\phi$, but as $\Phi$ increases, the creation of new obstacles is limited by already existing ones.

If a volume, v , is associated with each obstacle within which no new obstacle can form, then a balance of the number of obstacles can be set up.

$$\frac{dN_z}{dt} = N_o \sigma_B \phi \{1-vN_z\}$$

where $\sigma_B$ is the cross section for the production of a depleted zone and $N_o$ is the atomic number density. Upon integration, the equation yields

$$N_z = \frac{1}{v} [1-\exp(-N_o \sigma_B v \Phi)]$$

Hence, if $\sigma_i$ is proportional to $N_z^{1/2}$

$$\sigma_i = A[1-\exp(-B \Phi)]^{1/2}$$

where A is proportional to $1/v^{1/2}$ and $B = N_o \sigma_B v$.

Makin and Minter also investigate the idea suggested by Seeger that all obstacles will have the same activation energy for a dislocation to cut through them, i.e., the obstacles are of the same size. The saturation theory predicts that after a considerable irradiation, obstacles with a range of sizes will be present. For samples studied in the as-irradiated condition there was good agreement with Seeger's theory.

However, after mild annealing treatments, $\sigma_i$, which is proportional to the $\tau_o$ of Seeger, is not as temperature sensitive as in the as-irradiated condition.

These results help to validate the saturation theory because they suggest that there is a range of barrier sizes. At low temperatures those barriers with small activation energies will impede dislocation motion while at higher temperatures they will be transparent to dislocations (they can be overcome by thermal oscillations alone). On annealing, the obstacles with a low activation energy and, consequently, a small size will disappear first. This results in a rapid reduction in temperature sensitivity of $\sigma_i$, as is observed.

Up to this point it has not been discussed why the yield stress is expected to have a square-root dependence on dose. In a study by Tucker and Wechsler (7) the functional dependence of yield stress on dose is examined in detail. Niobium, a bcc metal, was used as a subject for the study.

The planar dispersed barrier model is used to explain the functional dependence of yield stress on dose. This model suggests that the defect clusters are barriers to slip dislocation motion on the slip plane. The model is tested by comparing its predictions directly with transmission electron microscope (TEM) observations. Niobium is well-suited for this study as the radiation-produced defect clusters are readily visible in TEM micrographs.

In developing the planar dispersed barrier model the interaction between dislocation lines and barriers is scrutinized. Under the action

of a shear stress, $\tau$, the force, F, on an obstacle created by a dislocation line pressing against it is

$$F = \tau b \bar{\ell}$$

where b is the Burgers vector of the dislocation line and $\bar{\ell}$ is the average interbarrier spacing. To arrive at the equation in terms of $\sigma$, recall that $\tau = \sigma/2$ for a polycrystalline, equiaxed specimen.

$$\sigma = 2\tau = 2F/b\bar{\ell}$$

The dose dependence of the yield stress enters through the dose dependence of $\bar{\ell}$.

From the conclusion that unirradiated (U)- and irradiated (I)-barriers act jointly, the theory can be developed further.

$$\sigma = 2\bar{F}/b\bar{\ell}$$

where $\bar{F}$ is an effective critical force for a dislocation line to cut through a barrier. Also, $\bar{\ell}$ can be expressed as

$$\bar{\ell} = 1/\sqrt{n_u d_u + n_i d_i}$$

where $n_u$ and $n_i$ are the density of U- and I-barriers, respectively, and $d_u$ and $d_i$ are the sizes of U- and I-barriers, respectively. Therefore,

$$\sigma = 2\bar{F} \, (n_u d_u + n_i d_i)^{1/2}/b$$

Further, reasoning that $\sigma = \sigma_u$ when $n_i = o$,

$$\sigma^2 = \sigma_u^2 + 4\bar{F}^2 \, (n_i d_i)/b^2$$

The final step in the development of the planar dispersed barrier model is to take into account the size distribution of the defect clusters, $I_c$.

$$I_c = \int_0^\infty n' \, d_i \, d \, d_i$$

where $n'$ is the defect cluster density per unit size interval. $I_c$ can then replace $n_i \, d_i$ in the equation for $\sigma^2$.

$$\sigma^2 = \sigma_u^2 + 4\bar{F}^2 \, I_c/b^2$$

This is, strictly speaking, the correct form of the equation with the dose dependence entering implicitly through $I_c$.

If, however, it is assumed that the density of the defect clusters increases linearly with $\Phi$ and that there is no change in size distribution an explicit function of $\Phi$ can be determined. The above assumptions basically ignore the saturation effect. $d_i$ can be replaced by $\bar{d}$, a mean defect cluster size independent of $\Phi$ and the cluster density can be expressed by

$$n = n_o \, \sigma_c \, \Phi$$

where $n_o$ is the atomic density and $\sigma_c$ is the cross section for producing a defect cluster. Then,

$$\sigma^2 = \sigma_u^2 + 4\bar{F}^2 (n_o \sigma_c \Phi)/b^2$$

Again, this is only correct for low doses before the saturation effect becomes apparent.

By conducting annealing studies, the nature of the defect clusters can be inferred. F. A. Nichols (8) looks at the recovery of radiation damage in ferritic steels. The defect aggregates are characterized as being groups of vacancies in agreement with Seeger. This point is required to explain the defect clusters' persistence upon annealing up

to temperatures of 300°C. As interstitials would be mobile at temperatures a great deal below 300°C, this seems like a plausible argument.

Nichols suggests three different mechanisms for the annealing of the defect clusters. All three are characterized by an activation energy at or near that for self-diffusion in order to agree with experimental observations. The first model assumes that the defect clusters are removed by having individual vacancies leaving the voids and travelling to sinks such as dislocations, grain boundaries, and surfaces. The second model suggests that the clusters are annihilated by the self-diffusion-controlled climb of dislocations. Both are characterized by having an activation energy equal to that of self-diffusion but neither can account for the rapidity of the observed annealing rate.

The third model suggests that there occurs the migration of entire clusters. In the early stages there is a coalescing to form a few larger clusters; which would reduce the hardening. In the final stages the larger aggregates would be absorbed at grain boundaries, dislocations and surfaces.

The third model is asserted to be practical one because it is assumed that the clusters migrate by the mechanism of surface diffusion. Atoms diffuse along the vacancy cluster (void) surface from the leading to the trailing edge. By having the migration occur by surface diffusion, the annealing rate would be increased to the point where theory and observation would agree and the activation energy would be only slightly less than that for self-diffusion. The rate of annealing would increase

because the entropy term of the diffusion coefficient would be much larger allowing for a greater lattice diffusivity.

The previous discussion has shown that neutron irradiation produces vacancy defect clusters which account for radiation hardening. Further, the planar dispersed barrier model is the theoretical basis for the impedance of dislocation by defect clusters. And, finally, there is a saturation effect which reduces the hardening rate at high neutron fluences.

## Radiation Embrittlement

Radiation embrittlement is another phenomenon associated with the neutron bombardment of metals. Wechsler (9) discusses the reduction in the load bearing capacity of irradiated metals. A note should be made here that the following points are applicable to many materials, including RPV steels.

To investigate the problem of radiation embrittlement there must be a clear understanding of what is meant by brittleness and by ductility. The two quantities are mutually exclusive to the extent that a material which is completely brittle shows no ductility and vice versa. The ductility of a metal is a measure of its ability to undergo plastic deformation before fracture.

Ductility has several measures including uniform elongation and reduction in area from tensile tests and the ductile-brittle transition temperature from notched bar impact tests.

Uniform elongation occurs in a tensile test up to the point where work hardening can no longer compensate for a localized reduction in area.

The uniform elongation is a measure of how much strain the metal can tolerate before work hardening no longer compensates for the stress increase due to localized reductions in area. After this point is reached, plastic instability is a result which leads to fracture.

Reduction in area, RA, is a measure of how much the cross sectional area of the tensile sample gage length decreases from its initial, unstrained value to its final, fractured value. It is represented by a simple equation

$$RA = (A_o - A_f)/A_o$$

where $A_o$ is the initial cross sectional area and $A_f$ is the final cross sectional area of the fractured surface.

The ductile-brittle transition temperature, DBTT, is, in principle, the temperature above which the metal behaves in a ductile fashion and below which it behaves in a brittle fashion. In actuality, there is a narrow temperature band over which the transition takes place. The DBTT is characteristic of RPV steels and will be discussed in greater detail further on.

Wechsler (9) discusses the effects of neutron irradiation on these measurements. Uniform elongation decreases upon irradiation while the reduction in area changes only slightly, if at all. Sometimes there is an argument as to whether or not embrittlement actually takes place since RA is not greatly affected. However, the decrease in uniform elongation shows that a reduction in load bearing capacity has taken place and, thus, a type of embrittlement has occurred.

The decrease in the uniform elongation is brought about by the premature onset of plastic instability. The instability is attributed to an observed inhomogeneous coarsening of slip. Coarseness in slip is characterized by local regions undergoing severe strains while the rest of the gage length may not. The elongation in these localized regions may be large but the strain averaged over the entire gage length would be low. The heavily strained regions reach a point of plastic instability and fail, bringing about the decrease in uniform elongation.

In turn, the coarsening of slip is surmised to be caused by dislocation channeling (7,9,10). Dislocation channeling occurs in many post-irradiated metals when radiation-produced defect clusters are removed by slip dislocations which are set in motion along a favorably oriented slip plane. Once the defect clusters are removed, subsequent slip occurs in the barrier free region in preference to the nucleation of slip on new bands in the adjacent crystal. Dislocation motion is easier once a region has been cleared of obstacles, allowing further deformation to take place in that region.

The mechanism suggested (7,9,10) for barrier removal in the incipient channel is adiabatic heating. The slip lines are formed very rapidly with a release of stored elastic energy. This release of energy, if preferentially deposited near the defect clusters, would allow localized annealing to take place, thus destroying the clusters.

The effect of neutron irradiation on the DBTT is also important with respect to RPV steels. The DBTT will first be defined in terms of

an unnotched tensile test and then corrections will be made for the conditions of the notched impact test.

The mechanism for the increase in the DBTT upon irradiation is usually explained in terms of the Ludwick-Davidenkov criterion (9,11,12). For the tensile test two stresses are considered; $\sigma_y$ and the cleavage fracture stress, $\sigma_c$. The criterion assumes that the material will be brittle or ductile depending on whether $\sigma_c$ or $\sigma_y$ is reached first upon increasing the load. $\sigma_c$ is assumed to be relatively independent of test temperature, strain rate, and microstructure. $\sigma_y$ increases rapidly with decreasing test temperature and it increases upon irradiation. Figure 1 represents this situation schematically. Thus, if the DBTT is measured at the intersection of the two curves it will increase upon irradiation by the amount $\Delta T$ because the intersection of the two curves will be shifted to the right. Therefore, since the increase in yield stress is due to radiation hardening, the DBTT shift can also be accounted for by radiation hardening.

A brief explanation by Olander (4) sheds further light on why there is neither expected nor observed to be an increase of $\sigma_c$ upon irradiation. Looking at two equations from the Cottrell-Petch theory of brittle fracture provided the basis for the argument.

$$\sigma_y = \sigma_i + k_y d^{-1/2}$$

and

$$\sigma_c = 2G\gamma d^{-1/2}/k_y$$

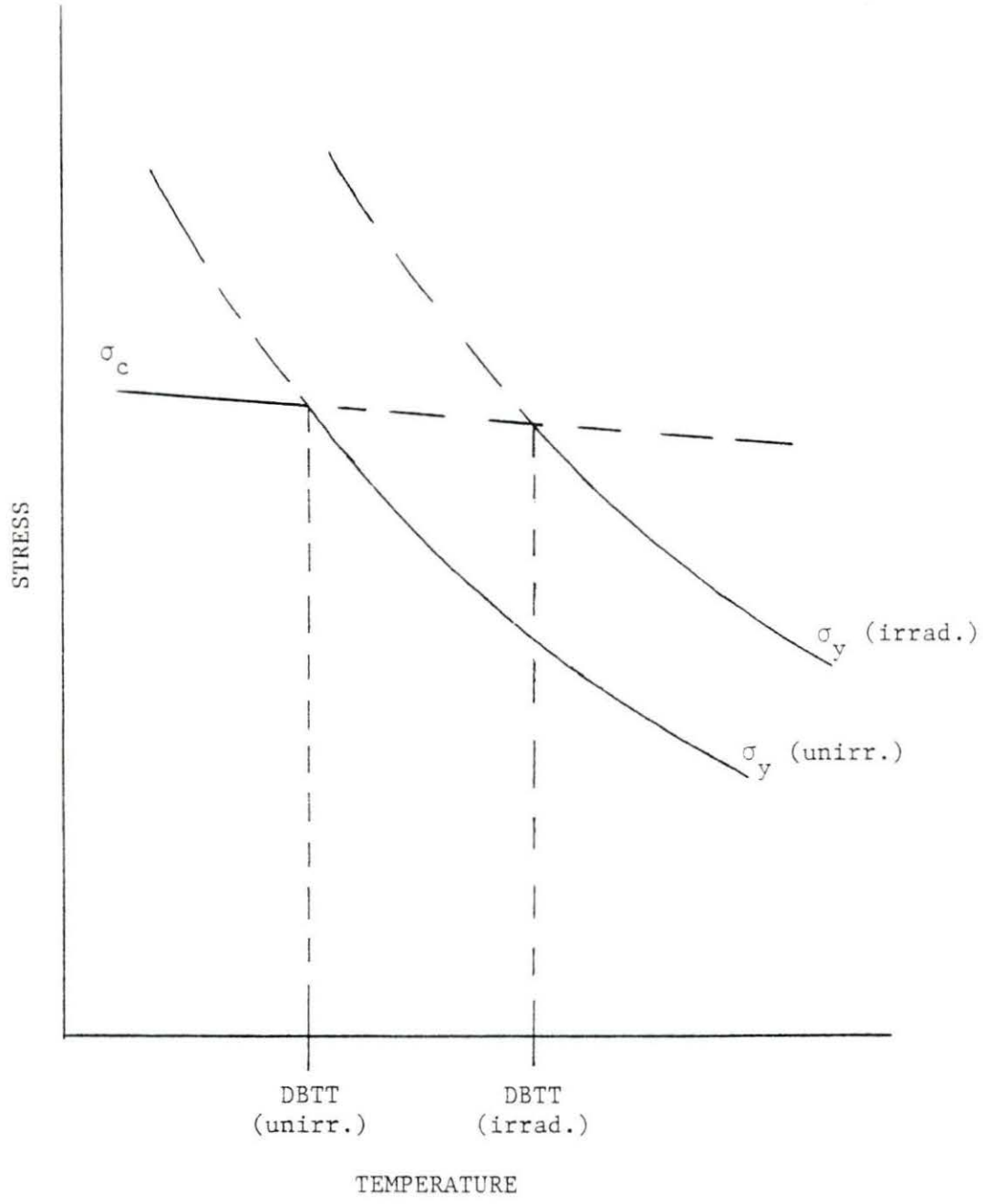


Figure 1. Schematic diagram of the Ludwik-Davidenkov criterion

where $k_y$ and d are defined as before, G is the shear modulus, and $\gamma$ is the surface energy related to crack propagation. The effect of radiation on the DBTT can be explained by referring to the above two equations.

The parameter $k_y$ depends on the stress required to unpin dislocations which, since bcc metals are already strongly pinned by impurities, is not sensitive to radiation in RPV steels. Thus, $\sigma_c$ will not be greatly affected by neutron irradiation.

However, $\sigma_i$ is quite sensitive to radiation as discussed before. As a consequence, the yield stress will increase upon irradiation.

Both results agree with the Ludwik-Davidenkov criterion and with experimental observation.

A note should also be made of the effects of a notch-impact test on the DBTT relative to a tensile test. In particular, the Charpy V-notch impact test is of interest because it is used quite often in studying RPV steels.

There are two main differences between the Charpy test and a tensile test. The presence of the notch in the Charpy test leads to the presence of a triaxial stress state compared to a uniaxial stress state in the tensile test and the strain rate is much higher in a Charpy test. These both have the effect of increasing the DBTT (11,13).

In addition to the increase in the DBTT neutron, irradiation also produces changes in another property measured by the Charpy V-notch impact test. The irradiation produces a decrease in fracture energy (absorbed energy for fracture) (9,14,15).

This decrease in the fracture energy is most significant in the ductile domain or upper shelf region. Above the DBTT a point is reached where increasing the test temperature no longer increases the fracture energy. This domain is called the upper shelf and the associated fracture energy is called the upper-shelf energy (USE). Fracture in this domain is 100% ductile.

The decrease in the USE is the equivalent (under the notched impact test conditions of high strain rate and triaxial stress state) to the decrease in area under the stress strain curve (for a uniaxial tensile test) (9). Thus, it is assumed that the decrease in the USE is another manifestation of the coarsening of slip upon irradiation. The effect of irradiation on a typical Charpy test transition curve is shown schematically in figure 2.

The discussion on radiation embrittlement has shown that the decrease in ductility (increase in brittleness) upon irradiation is due to the coarsening of slip caused by dislocation channeling. At least the dislocation channeling accounted for the decrease in uniform elongation in the tensile test and the decrease in USE in the Charpy impact test. However, no new mechanism was needed to account for the increase in the DBTT, as it could be explained by radiation hardening.

## In-Service Response of Reactor Pressure Vessels

During operation the reactor pressure vessel must be monitored so that its continued safe operation is assured even though the mechanical properties are degraded as a result of the radiation-produced defects

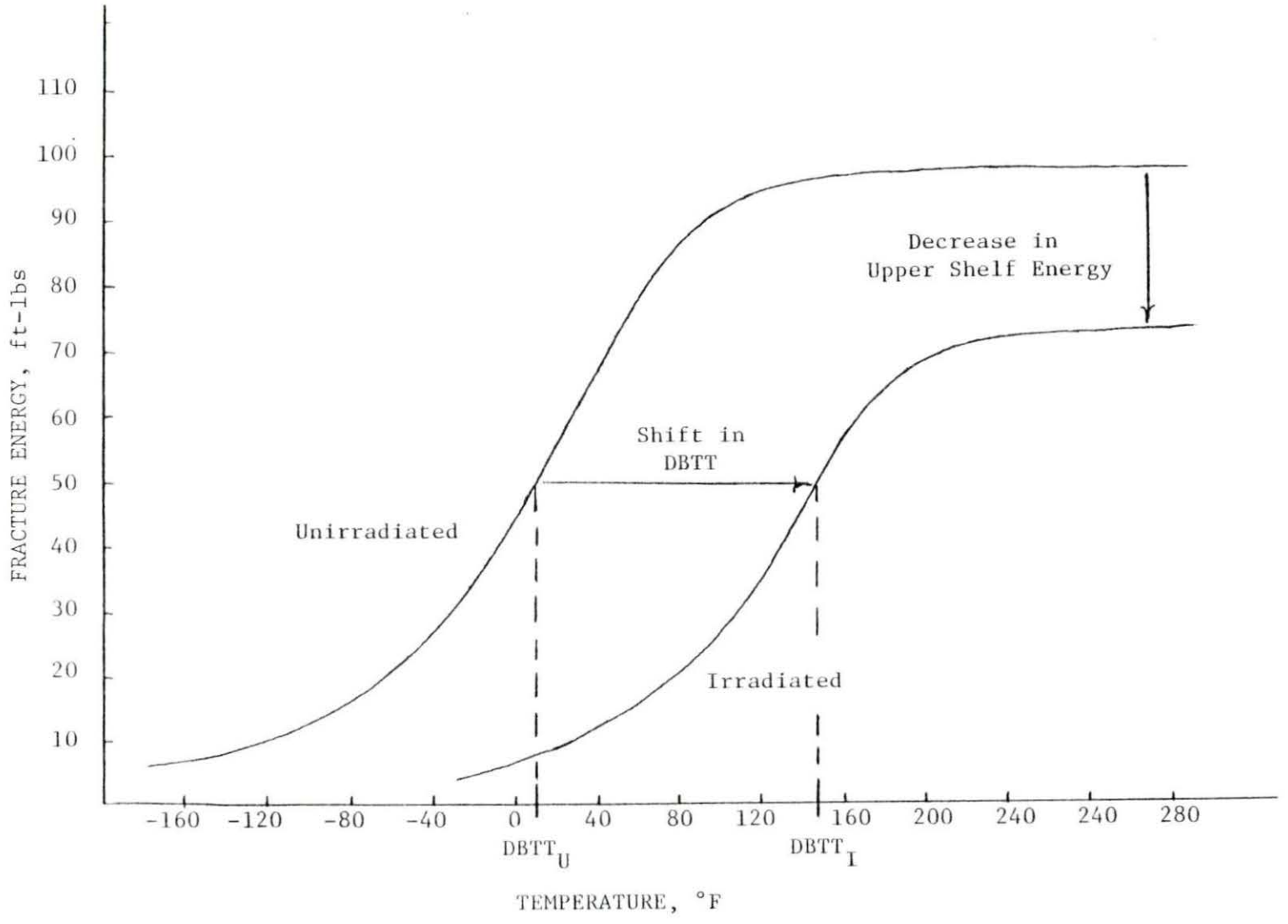


Figure 2. Schematic diagram of the changes in the Charpy impact test transition curve upon irradiation

(as discussed before). There are several standards which regulate the use of reactor pressure vessels and they include the Code of Federal Regulations (16,17), the ASME Boiler and Pressure Vessel Code (18), and various ASTM Standards (15,19).

The above regulations define the minimum mechanical properties allowed for continued safe operation of the plant. The mechanical properties cited usually involve the fracture energy as measured in the Charpy impact test, and the fracture toughness, as measured in linear elastic fracture mechanics, at a specific temperature (16,17,20). These requirements are involved mainly with the beltline material of the pressure vessel because it is this material which undergoes the greatest property changes upon irradiation. Strictly defined, the reactor beltline region is the shell material directly surrounding the effective height of the fuel element assemblies and any additional height of shell material for which the predicted adjustment of reference temperature exceeds 50 degrees F at the end of service life (16).

The reference temperature, $RT_{NDT}$, just mentioned is roughly the same as the ductile-brittle transition temperature, DBTT, defined for the Charpy V-notch impact test. In referring back to figure 2, $RT_{NDT}$ can replace, in a qualitative manner, DBTT.

$RT_{NDT}$ has a rather strict definition as well (18). A temperature, $T_{NDT}$, is chosen which is at or above the nil-ductility temperature as determined by a dropweight test. At a temperature not greater than $T_{NDT}$ plus 60 degrees F, the material must exhibit at least 35 mils of lateral expansion and a fracture energy not less than 50 ft. lbs.

(both of which are measured in the Charpy impact test). If those requirements are met then $T_{NDT}$ is $RT_{NDT}$.

If the aforementioned requirements are not met, additional tests must be conducted to determine the temperature, T, at which they are met. In this case, $RT_{NDT}$ is equal to T minus 60 degrees F. Finally $RT_{NDT}$ must be determined for the base plate material, the weld metal, and the heat affected zone associated with the weld.

In the determination of $RT_{NDT}$ a minimum upper shelf energy, USE, for the reactor pressure vessel is required. The limit is a minimum USE of 50 ft lbs (with the 35 mil lateral expansion requirement being roughly equivalent to it). At present, the USE must be 50 ft lbs or greater because the $RT_{NDT}$ criterion becomes inoperative when the USE falls below that level. It should be noted here that the 50 ft lb level is an arbitrary limit and that the Nuclear Regulatory Commission (NRC) is considering a revision which would reduce the limit to 30 ft lbs. The motivation for this is that some plants are approaching the 50 ft lb level and may soon have an undefined $RT_{NDT}$ (21).

Having a definable $RT_{NDT}$ is important because it is used to determine the pressure-temperature operating limits of the reactor system. The method for determining these limits is given in Appendix G of Section III of the ASME Boiler and Pressure Vessel Code (20). The Appendix presents a procedure for obtaining the allowable loading limits for ferritic pressure retaining materials. The determination is based on the principles of linear elastic fracture mechanics.

Since the concept of fracture mechanics is so important to understanding the ideas of Appendix G it is briefly described here. When using fracture mechanics (6,22) it is assumed that all structures contain certain flaws (cracks) of various sizes. The resistance to crack growth (sometimes called toughness or fracture resistance) and an attempt to quantify that resistance are the main concerns of fracture mechanics. The response of many different kinds of cracks can be described but Appendix G is solely concerned with a surface crack having a sharp tip.

The local stresses near the tip of a surface crack depend on the product of the nominal stress and the square root of the crack depth. This dependence is described by what is known as the stress intensity factor, K. K is a function of the applied load, the crack size, and the dimensions and shape of the body. Also, K is usually given in units of ksi $(\text{inches})^{1/2}$.

Since K describes the stress distribution around the crack tip and since the intensity of the stress field determines whether or not a crack will propagate, the value of K is a measure of the material's resistance to crack growth. The critical value of K, where the crack becomes unstable and grows catastrophically, is called the fracture toughness of the material.

The final point to be made on crack propagation is the manner in which a crack grows or opens up. There are three modes of crack growth including the opening mode, the forward shearing mode, and the edge sliding mode. The modes are often referred to as mode I, II, and III,

respectively. Of major concern to this discussion is the mode I form of crack propagation.

In Appendix G the mode I stress intensity factor, $K_I$, is determined for each loading component of the reactor pressure vessel (20). The summation of the $K_I$ values is then compared to a reference value, $K_{IR}$, where $K_{IR}$ is the fracture toughness of the material involved. It should be noted here that $K_{IR}$ is dependent on the temperature of the material.

In defining the operating limits of the reactor pressure vessel the value of $K_{IR}$ is related to the temperature of the vessel and to $RT_{NDT}$.

$$K_{IR} = C_1 + C_2 \exp[\, C_3(T-RT_{NDT}-160^{\circ}F)\,]$$

where $C_1 = 26.78$ ksi $\sqrt{\text{inches}}$

$C_2 = 1.233$ ksi $\sqrt{\text{inches}}$

$C_3 = 0.0145$ (degrees F)$^{-1}$

and T = the temperature of the pressure vessel in degrees F.

Used in the development of $K_{IR}$ is a maximum postulated defect which is, in this case, a sharp surface crack. The crack has a depth of 1/4 the wall thickness. Due to the safety factors involved the prevention against non-ductile fracture is assured even if the defect is twice as large, in linear dimensions, as the one assumed (20).

When considering the pressure vessel (excluding discontinuities at flanges, etc.) the main loadings come from the system pressure and from the thermal stress due to the thermal gradient during startup and

shutdown. A safety factor of 2 is introduced into the calculation of the $K_I$ value produced by the primary system pressure. By taking those factors into account and by summing up the $K_I$ values, the following inequality results

$$2K_{IM} + K_{It} < K_{IR}$$

where $K_{Im} = M_m$ x the membrane stress (induced by the system) and

$K_{It} = M_t$ x the temperature difference through the wall of the pressure vessel in degrees F.

$M_m$ and $M_t$ depend on the wall thickness and can be determined from graphs in the Appendix (20).

Since $RT_{NDT}$ changes during the lifetime of the reactor (along with the other mechanical properties) and since the allowable pressure-temperature limits change with it, a materials surveillance program is needed to measure these changes. Under a surveillance program, fracture toughness data are obtained through periodic removal of material specimens from the reactor. The specimens are subjected, as nearly as possible, to the same neutron and temperature environment as the reactor vessel (17). Charpy samples and tensile samples are included in the surveillance capsule to monitor the property changes.

Most present surveillance programs have 5 surveillance capsules with a typical withdrawal schedule as follows (17). The first capsule is withdrawn when the predicted shift in $RT_{NDT}$ is 50 degrees F or at 1/4 of the service life, whichever is earlier. The second capsule is withdrawn approximately 1/3 of the way between the first and the fourth, while the third capsule is withdrawn at 2/3 of that interval. The fourth capsule

is withdrawn at 3/4 of the service lifetime, the fifth capsule being on standby.

When conducting surveillance programs there are several important factors which need to be considered if the program is to be a successful one. Among these are the selection of appropriate steels, careful neutron dosimetry (to permit correlation from the specimen location to the reactor vessel wall) and proper temperature characterization.

The selection of appropriate steels may be the most important factor. In a conservative design the limiting steel, i.e., the one most sensitive to neutron irradiation, must be included in the surveillance capsule. This is a necessary but difficult task because there is a variation of irradiation response from steel-to-steel and even from heat-to-heat of the same steel (9,21). The regulations stipulate that the limiting steel will judge the pressure vessel operating limits (18). If the radiation response of the steels involved is not known beforehand, care must be taken to include samples of basically all the steels .

To determine the neutron environment each capsule contains neutron dosimeters (activation foils). Two examples of reactions used for activation analysis are $Fe^{54}$ (n,p) $Mn^{54}$ and $Ni^{58}$ (n,p) $Co^{58}$ (21). Computer physics codes are used to predict the actual neutron environment at the wall compared to that at the surveillance capsule.

Since the temperature can also affect the magnitude of radiation induced changes, it too is monitored (21). Since it is not practical to continuously monitor the temperature, low melting point elements or eutectics are included. These provide evidence of the maximum exposure

temperature. Some examples are: 97.5% Pb, 2.5% Ag (304 degrees C melting point) and 97.5% Pb, 1.75% Ag, and 0.75% Sn (310 degrees C melting point).

The importance of having a surveillance program of adequate scope has been pointed out with a problem that has arisen because of the extra radiation sensitivity displayed by some steels. The sensitivity is caused by the presence of some trace elements (most notably copper and phosphorous) (23-28). A large portion of the problem involves weld metal which was not originally thought to be limiting because of good initial properties. Later, however, they were found to be overly sensitive. The presence of copper and phosphorous dramatically increase the magnitude of both the change in $RT_{NDT}$ and the decrease in USE (23,24,29,30) and, although it was discovered in the late 1960s, the cause of the effect has not been definitely established (23,24).

The NRC has taken into account the inadequacy of early surveillance programs by issuing Regulatory Guide 1.99 (26). When adequate surveillance data are not available, empirical equations furnished in this guide are used to predict the changes in $RT_{NDT}$ and USE based on the amount of copper and phosphorous present and the fluence. As an example, for the shift in $RT_{NDT}$:

$$A = [40 + 1000(\%Cu - 0.08) + 5000(\%P - 0.008)](f/10^{19})^{1/2}$$

where A = predicted adjustment of reference temperature in $^{o}F$

f = fluence in neutrons per $cm^2$, E > 1 MeV

%Cu = weight % of Cu

and %P = weight % of P.

If the copper amount is less than 0.08%, then 0.08% is to be used in the equation and if the phosphorous amount is less than 0.008%, then 0.008% is to be used. The equations given in Regulatory Guide 1.99 are for nominal irradiation temperatures of 550°F, the operating temperature of the reactor pressure vessel.

Again, the magnitude of the trace element effect is relatively large. Predictions suggest that the change in $RT_{NDT}$ could be more than 400 degrees F by the end of the service life for some sensitive steels (more than double that for steels with low amounts of trace elements) and the drop in USE could also be doubled (24,25).

As mentioned before, the mechanism for the enhancement of radiation embrittlement in the presence of trace elements is not completely understood. However, the prevalent model suggests that radiation-produced defects (and defect clusters) are stabilized against annealing by the presence of trace amounts of copper and phosphorous.

Two variations on the above model are suggested by Wechsler (23) and Smidt and Steele (24). Wechsler suggests that when trace elements are present in sufficient quantities they can migrate to the defects and stabilize them so that they cannot anneal away during irradiation at the elevated temperatures. Smidt and Steele suggest that the nucleation of defect aggregates is modified so they are, in effect, increased in number. Rather convincing evidence is presented in both papers to show that there is somehow an interaction between copper atoms and vacancies to form a more stable defect. The following discussion is mainly concerned with copper rather than phosphorous.

The first evidence cited demonstrates that vacancies are involved because the trace element effect is only apparent at temperatures where vacancies are mobile (392 degrees F and up (24)). Also, no effect is seen at irradiation temperatures of 250 degrees F or lower, i.e., the radiation response is the same for high and low copper steels at the lower irradiation temperatures. Thus, since interstitials are still mobile at the lower temperatures they cannot be responsible for the interaction. It should be noted here that copper is a substitutional impurity.

Second is the fact that, in general, as the irradiation temperature increases the irradiation produced hardening is decreased as dynamic recovery occurs. Almost all damage undergoes dynamic recovery, in the materials with small amounts of trace elements, at reactor operating temperatures ($550^{\circ}$F). However, steels with large amounts of trace elements do not show complete dynamic recovery; thus, a more stable defect has been formed.

Finally, Smidt and Steele (24) point out that in annealing experiments they conducted, the materials high and low in residual elements have similar annealing responses. Both types of material tend to undergo complete recovery to the pre-irradiation hardness value after 1 hour at the same temperature (1024 degrees F, 550 degrees C). Also, the similarity of the recovery behavior suggests that any difference in irradiation response is most likely one of magnitude of dynamic recovery rather than the formation of any new type of defect aggregate. Again,

this points out the suspected stabilizing effect that copper has on vacancy aggregates.

Most of the steels that exhibit this trace element effect are weld metals (21). The high copper weld metals have been identified as life limiting factors for many reactors (21, 25). This is not completely surprising because significant amounts of copper can be introduced by submerged arc welding (SAW) process. Many welds in RPV's are formed by SAW. In the submerged arc welding process a consummable electrode is used and this electrode is often lightly coated with copper to provide some protection from rust and to ensure good electrical contact for good weld characteristics (31).

The two major problems which arise from the trace element effect are what can be done to prevent the problem from recurring in reactors to be built and what can be done to correct the problem for reactor pressure vessels which are already constructed and which have high copper levels.

The simplest approach to avoiding the trace element effect is to control the amount of residual elements. Significant improvement in radiation response is attained by restricting copper and phosphorous contents (32-35). Because of this, vessel manufacturers have been controlling the amount of copper and phosphorous since 1971 (32).

Improved steelmaking practice was needed to control the copper content to 0.10% max and 0.012% P max (the levels above which a trace element effect becomes readily apparent). A major reduction in radiation sensitivity was achieved in commercial A533 B plates and weld metal

through the reduction of copper and phosphorous contents to these levels (32). It is noted here that optimum steelmaking practice can reduce the copper and phosphorous contents even lower but this further reduction does not greatly improve radiation resistance (33). Also, the cost of the pressure vessel is not significantly increased by the use of improved steel making practice when compared to the total cost of the pressure vessel (34).

In discussing what can be done about those reactors already afflicted with the problem, two options are being considered; a thermal annealing treatment of the pressure vessel or an essentially complete volumetric fracture mechanics examination of the beltline material which conservatively demonstrates that an adequate safety margin for operation is maintained. Both options are provided for in the Code of Federal Regulations (16).

The first option, a thermal annealing treatment, has received more attention and is looked at in greater detail here. If thermal annealing is conducted several things must be considered (16,19). The recovery upon annealing must be determined by testing additional specimens withdrawn from a surveillance capsule. Those specimens must be subjected to the same time at annealing temperature as the pressure vessel (the results provide the basis for an adjusted reference temperature after annealing). The response to subsequent irradiation after annealing must also be taken into account. Both the annealing response and the re-irradiation response are hard to predict because the mechanism for the trace element effect is not well-known.

Two annealing alternatives are presently being considered: annealing at 343 degrees C (650 degrees F) or at 399 degrees C (750 degrees F) (29). The 343 degrees C heat treatment was selected as the maximum temperature at which nuclear or pump heating could be employed. The major advantage of this first alternative is that the reactor coolant and, more importantly, the core internals are left in place. The 399 degrees C treatment was chosen as an achievable temperature if auxiliary heaters are employed. This second alternative is advantageous because greater properties recovery can take place by virtue of the higher temperature, but, it is disadvantageous because the core internals, as well as the reactor coolant, must be removed (29). The removal of the internals and the coolant would add to the complexity of the problem.

The 343 degrees C treatment produced a high degree of recovery (between 62 and 100%) in the USE but only limited recovery in $RT_{NDT}$ (between 22 and 29%) after 168 hours at temperature. However, the re-irradiation properties (to a fluence of $3.6 \times 10^{18}$ n/cm$^2$, E > 1 MeV) were either poorer or the same as notch ductility observed after the first cycle of irradiation (with a fluence of $1 \times 10^{19}$ n/cm$^2$, E > 1 MeV). The 168 hour treatment was chosen as the optimum time because annealing for longer times does not significantly increase the recovery of pre-irradiation properties (30).

The 399 degrees C, 168 hour, treatment produced 100% recovery of USE and 70% recovery of $RT_{NDT}$. The steel showed good re-irradiation

properties (at a fluence of $7.2 \times 10^{18}$ n/cm$^2$, E > 1 MeV), with notch ductility properties better than that found after the first irradiation cycle (with a fluence of $1 \times 10^{19}$ n/cm$^2$, E > 1 MeV) (29).

The second alternative, annealing at 399°C, shows a good deal of promise and is a possible solution to the problem concerning what is to be done about the pressure vessels afflicted with high copper and phosphorous contents (29,30).

The problems associated with the in-service response of reactor pressure vessels have been addressed at length. Included in the discussion were the various regulations which assure adequate safety margins for operation. The need for a good surveillance program, in order to monitor the changes in mechanical properties, was also demonstrated. Finally, the serious problem arising from the trace element effect was discussed in detail.

# EXPERIMENTAL PROCEDURE

The purpose of this study is to investigate the change in mechanical properties undergone by pressure vessel steel subjected to a neutron fluence of approximately $1 \times 10^{18}$ $n/cm^2$, $E > 1$ MeV. The change in mechanical properties is characterized by the difference in microhardness between unirradiated and irradiated samples. Annealing studies are also conducted in order to determine an activation energy for the hardness recovery from the irradiated to the annealed condition.

## Sample Preparation

The specimens used are Charpy bar halves from an actual surveillance program. That is, the samples were broken in a Charpy test, but are still usable for hardness tests. The halves are sectioned into quarters using a cutoff wheel mounted on a milling machine. Each of the quarters is then considered to be a test specimen. The quarters measure approximately 4mm x 4mm x 27mm and approximately 100 diamond pyramid hardness tests can be made on one 4mm x 27mm face.

In particular, the Charpy bar halves are from weld metal surveillance samples. This is appropriate material to study because, as mentioned in the section on in-service response of the reactor pressure vessels, the weld is usually the life limiting material in the pressure vessel. However, these samples are not completely homogeneous, i.e., they are not completely made of weld metal. This may seem to be contradictory since the Charpy impact tests conducted for the sur-

veillance program were supposed to measure the weld metal properties. There is no contradiction, however, because only the central portion of the Charpy bar containing the notch needs to be made of weld metal.

With this in mind, the Charpy bars were originally sectioned from the weld metal region so that the bar traversed the weld metal and had both its ends in base plate. The situation is shown schematically in figure 3. Three major regions are contained in each Charpy bar half: base plate, weld heat-affected zone, and weld metal.

After sectioning, the surface of the test specimen was polished to remove any surface defects (scratches, oxidation, etc.) and to facilitate measuring the hardness indentations. The ASTM Standard for diamond pyramid hardness testing (36) requires that the surface of the specimen be prepared so that the ends of the impression diagonals can be read with precision. The manner in which the hardness of the specimen is determined is discussed in detail in the next section.

The metallographic grinding and polishing for the unirradiated samples include 3 steps. For rough polishing, 320 grit silicon carbide (SiC) paper was used. This was followed by grinding with 600 grit SiC paper. Both grinding steps were undertaken on a motor-driven grinding wheel. The final step in the preparation was polishing with 0.3 micron alumina powder in a slurry of ethylene glycol and isopropyl alcohol. The slurry contained equal concentrations of the two liquids. The polishing was done on a motor-driven polishing wheel covered with a nylon cloth.

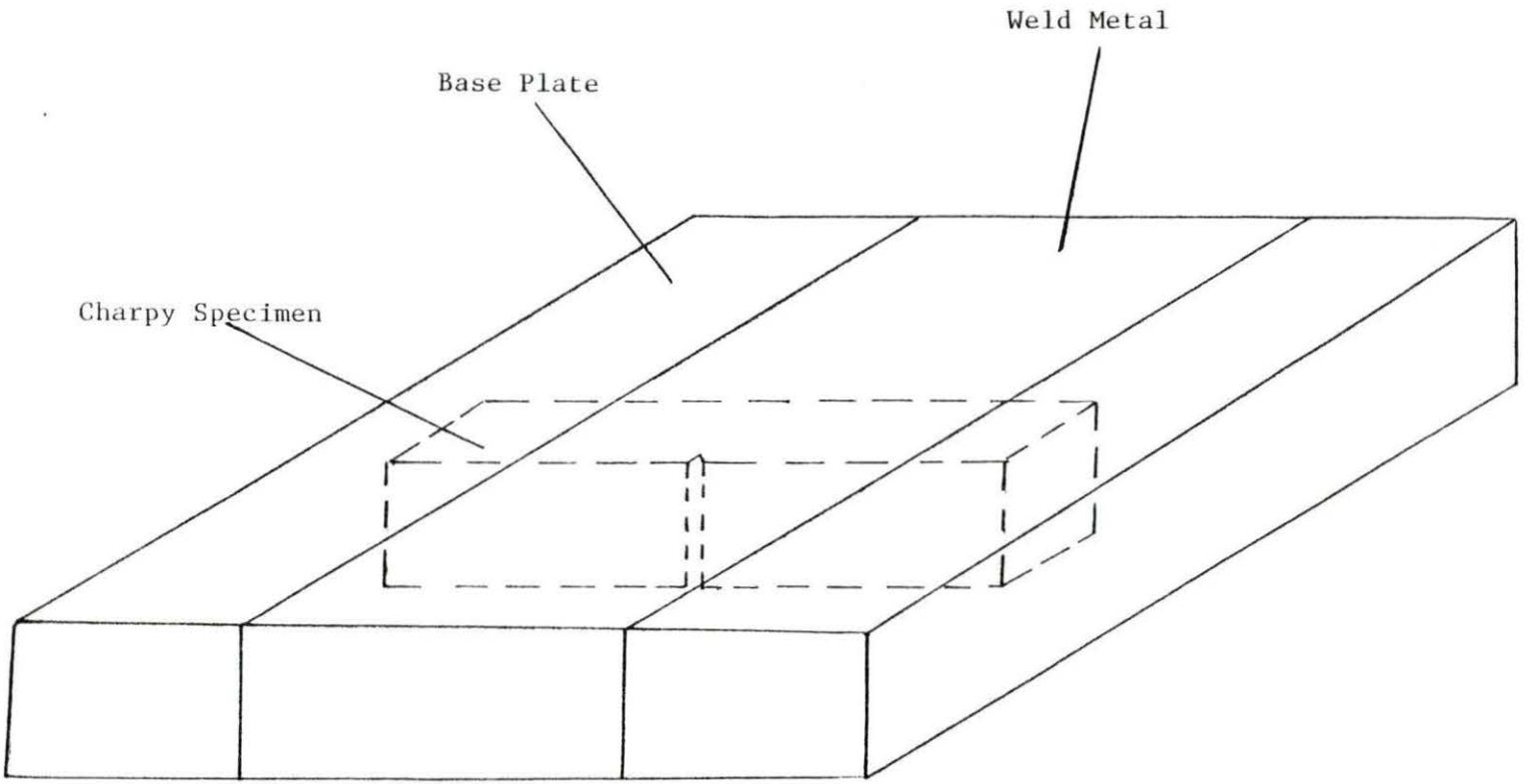


Figure 3. Schematic illustration of the cause of the Charpy bar heterogeneity

The same sequence of steps was used for preparing the irradiated samples. However, in order to minimize exposure to the hands, a semi-automatic grinder/polisher was used. Also, to reduce any problem with contamination the grinder/polisher was placed in a glovebox. For each step in the grinding and polishing, a new bowl containing the proper abrasive had to be inserted. Except for changing the bowls and setting the controls, the process was automatic.

The final step in the sample preparation process was a very light etch using a 6% Nital etchant (94% methanol, 6% nitric acid). The etching was done for a very short time, approximately 2 seconds, followed by a rinse with methanol. This amount of etching allowed the experimenter to delineate between the base plate, heat affected zone (HAZ), and the weld metal. Without the etching step it would not be possible to know which microstructure region was being tested.

## Microhardness Testing

The hardness of a material is a measure of that material's resistance to local indentation. Hardness is determined by releasing a load onto a material with an indenter of a specified geometry and then judging how hard or soft the material is by the size of that indentation.

This study uses the diamond pyramid test (also called the Vickers hardness test). The indenter associated with this test is a square-based pyramidal diamond (or sapphire) indenter having included face angles of 136 degrees (36). The hardness number associated with the test is the diamond pyramid hardness number and is referred to as the DPH of

the material. DPH is obtained by dividing the load in kilograms force by the surface area of the indentation in square millimeters.

The projected area of the indentation on the surface of the metal is a square. The diagonals of that square are then measured and averaged. The following equation is then used to calculate the hardness:

$$DPH = 2P \sin(a/2)/d^2$$

where P = load in kilograms-force

d = mean diagonal length in mm

and a = the included face angle of the indenter (136 degrees).

At this point it should be noted that hardness is a more complex mechanical property of a metal than, say, the yield stress. This is because of the triaxial stress state that exists underneath the indenter tip. Nevertheless, the hardness test is indicative of changes in the properties of metals (6) and, thus, is suited for this study.

To conduct the hardness tests a hardness tester was constructed using plans obtained from the Oak Ridge National Laboratory (37). Some modifications were made to the plans which allowed x and y translational motion of the indenter. This made it possible to conduct any number of hardness tests (up to several hundred) without removing the specimen holder. The push rod drive mechanism was also modified. A schematic diagram of the apparatus is shown in figure 4. The hardness tester can operate at temperatures up to 850$^{o}$C while the

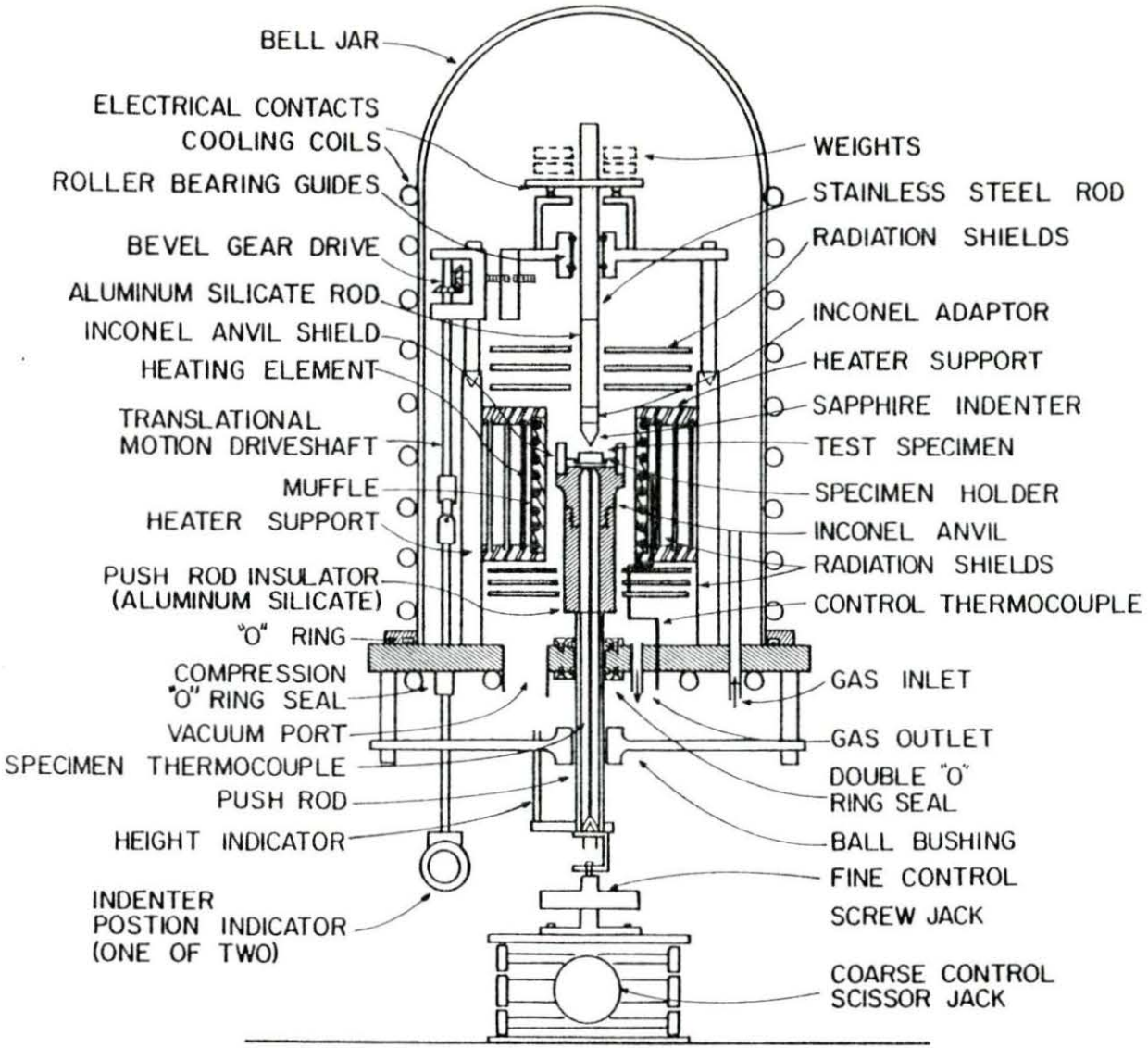


Figure 4. Schematic diagram of the elevated temperature microhardness tester

sample is under either vacuum or inert atmosphere, but only room temperature tests were conducted in this study.

The procedure for making a room temperature test is as follows. The specimen is raised to within 1/8 inch of the indenter using the coarse control for the push rod drive. The fine control is then used to raise the specimen against the indenter until the specimen supports the full load of the indenter plus added weights (2.045 $Kg_f$). After a prescribed time, approximately 13.5 seconds as measured by a stopwatch, the specimen is lowered to release the load. The time is measured from the moment the specimen supports the full load to the time the load is released. An electrical contact circuit with a light indicates when the load is being fully supported and when the load is released. Subsequent indentations are made by translating the indenter along the specimen. The whole process is done manually.

The application of the load must be done without shock or vibration (36). This is assured by a slow specimen-indenter impact speed, estimated to be in the range of 3 to 6 mm/min. Further, at these low speeds the effect of loading rate on the DPH obtained is very small (38).

Measuring the hardness indentation is the final step before calculating the DPH. In this step, a filar eyepiece (with a precision better than 0.5 microns) is used to measure the diagonal length. It is important at this point to make sure that each indentation is a good one. This is done by making sure that the indentation is approximately symmetrical and by focusing deep into the impression to determine that no irregularities are present on the surface of the

indentation. An asymmetrical indentation is often indicative of indenter misalignment and surface irregularities are indicative of a damaged indenter tip, both of which can affect the hardness value obtained.

The final step in assuring good hardness results involved calibrating the filar eyepiece used to measure the impressions. The filar eyepiece was calibrated to a standardized hardness block supplied by the Wilson Instrument Company. Supplied on the standard block were 5 rows of 5 indentations with an average diagonal length given for each row. The hardness impressions for each row were remeasured using the filar eyepiece. From these measurements an average diagonal length, $\bar{d}_c$, was calculated for each row and then compared to the actual average diagonal length (as determined by the Wilson Instrument Co.), $\bar{d}_a$. A correction factor, $F_i$, for the $i^{th}$ row was determined according to the following equation.

$$F_i = \bar{d}_a/\bar{d}_c$$

An overall correction factor, $F_o$, was then determined by taking the average of the five row correction factors. $F_o$ was then used in any hardness tests conducted by multiplying the measured diagonal lengths by $F_o$ ($F_o = 1.014$).

## Annealing Procedure

To determine the activation energy for the hardness recovery some annealing treatments had to be conducted. Included were both isochronal and isothermal annealing runs. Isochronal annealing runs

involve taking a test specimen and heating it up to the annealing temperature, $T_A$, then holding it at that temperature for some chosen time, and, finally, letting it cool down. Subsequent isochronal runs for that specimen are conducted at higher temperatures but with the time at temperature being held constant. The isochronal time at temperature for this study was 1 hour with the annealing temperature ranging from 293 degrees C to 510 degrees C in approximately 30 degree increments.

In isothermal annealing the annealing temperature remains constant but the time at temperature can vary from one run to the next. Two series of isothermal treatments were conducted with one at 415 degrees C and one at 445 degrees C.

A vacuum furnace assembly was constructed for the annealing treatments (see figure 5). The furnace was designed with two thermocouple probes which can variously be inserted or withdrawn from the heated zone (center) of the furnace. A stainless steel specimen holder was welded to thermocouple probe number 1.

The general procedure for isothermal and isochronal treatments was the same. The specimen was placed in the specimen holder after which the flange (through which the thermocouple probes pass) was bolted in place. The whole system was then put under a vacuum of approximately $2 \times 10^{-6}$ torr. Next, the furnace was brought up to the annealing temperature as monitored by thermocouple number 2 with the specimen in the withdrawn position (out of the heated zone). After the furnace reached the annealing temperature, the specimen was inserted into

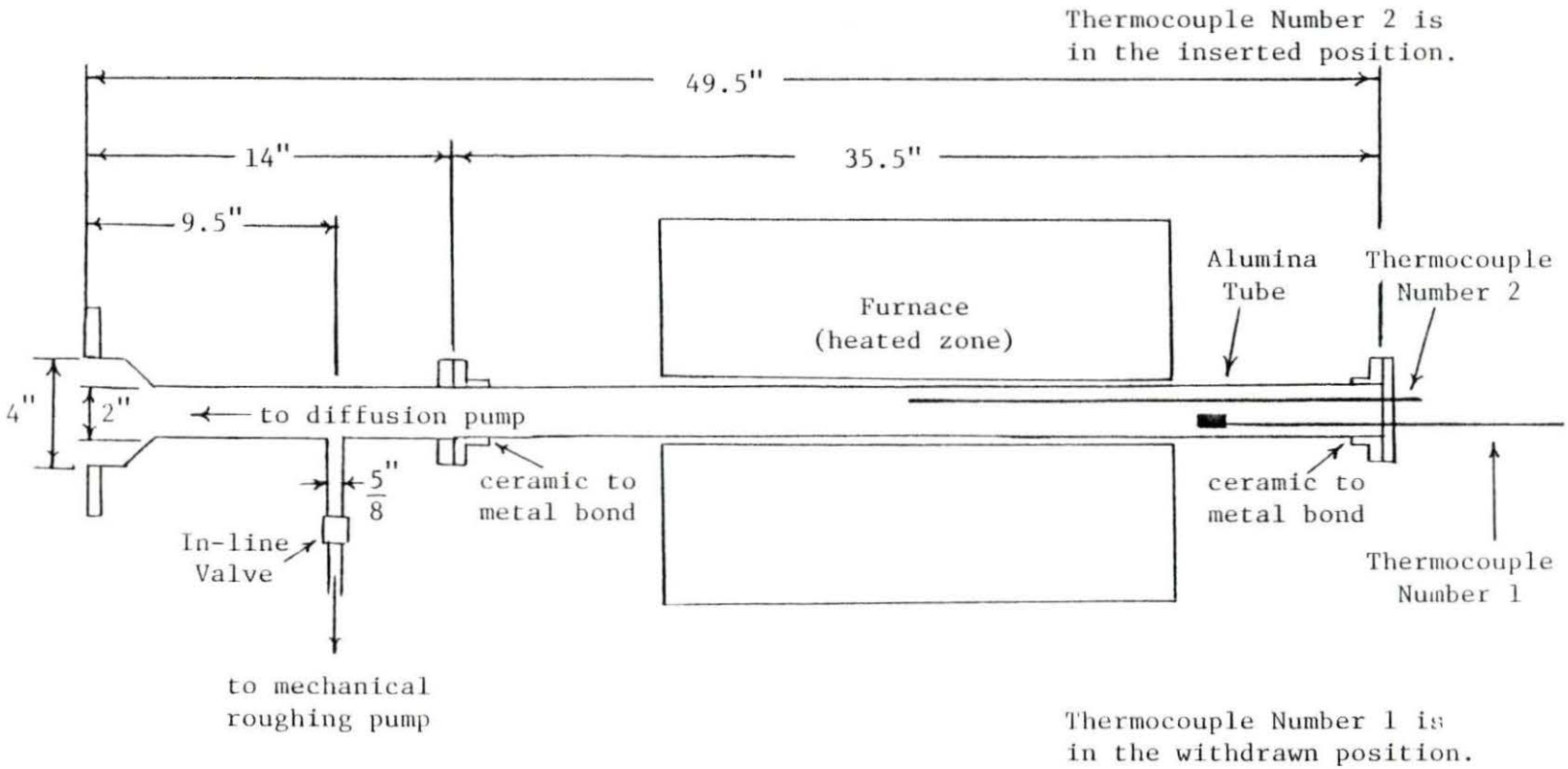


Figure 5. Diagram of the vacuum annealing furnace

the heated zone. The specimen took approximately 15 minutes to reach the annealing temperature at which the specimen was held for a predetermined time. After that time elapsed, the specimen was withdrawn from the heated zone. Again, all of this was conducted under vacuum.

The final step was a series of room temperature hardness tests on the weld metal to characterize its average hardness. Usually, 5 tests were conducted at this time.

The reason for inserting the specimen after the furnace is already at temperature and subsequently withdrawing it after the desired time at temperature has elapsed is simple. The reason is that the temperature versus time response of the specimen should resemble, as closely as possible, a step function. Even with the insertion and withdrawal the temperature-time response is not a step function.

Since the temperature-time response is not a step function, an equivalent time at temperature must be calculated for the heatup and cooldown of the test specimen. The idea is shown schematically in figure 6. An effective time at temperature is calculated for the lined regions in the figure. The total corrected time at temperature is the sum of the effective times at temperature and the actual annealing time (the nominal time while the specimen is actually at the annealing temperature).

The amount of recovery is proportional to the product $t \exp\left(-\frac{E_A}{kT}\right)$ (see discussion in RESULTS, Activation Energy Analysis) where t is the annealing time, $E_A$ is the activation energy for the recovery process, k is Boltzmann's constant, and T is the annealing temperature. With

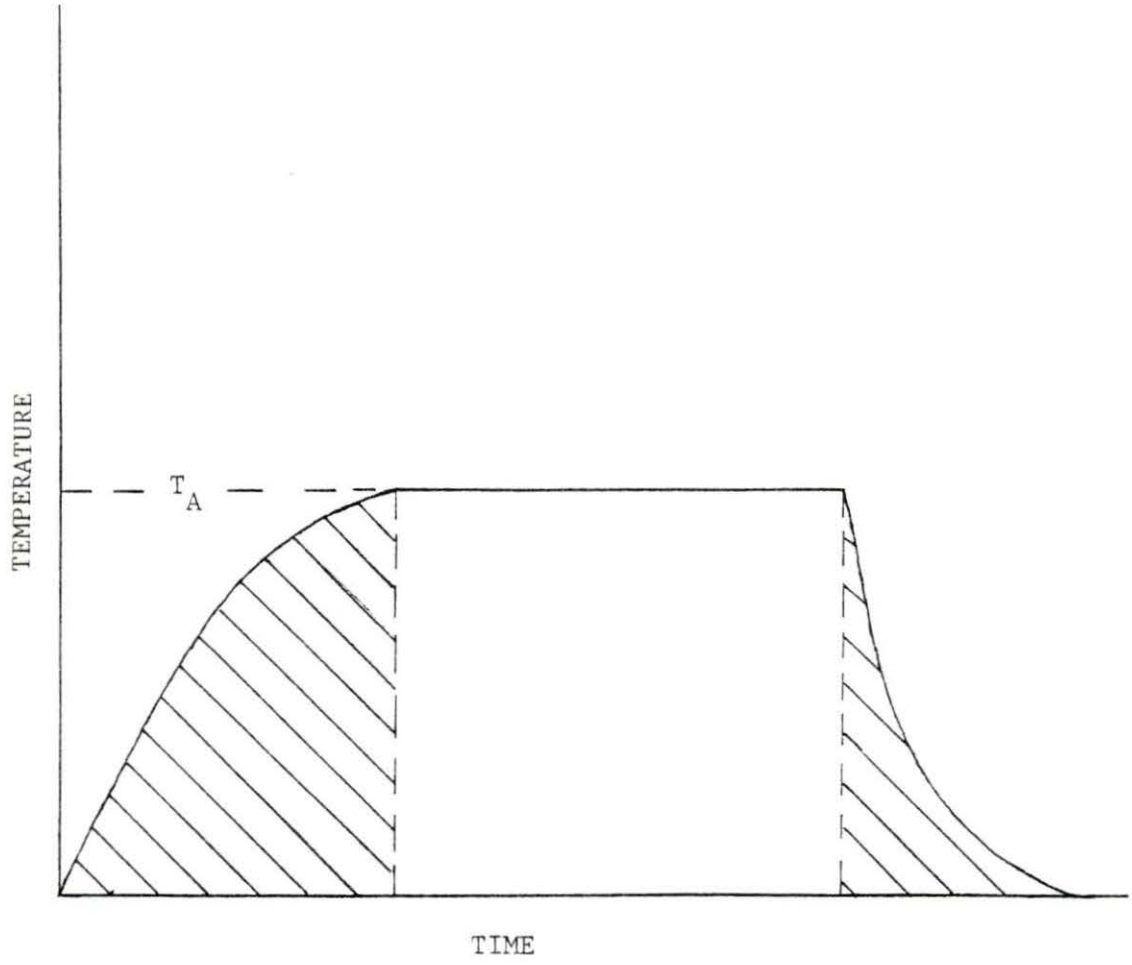


Figure 6. Schematic diagram of a specimen time-temperature response during annealing

this in mind, we can calculate an effective time at temperature, $t_{eff}$, in the following way:

$$t \exp\left(-\frac{E_A}{kT}\right) = t_{eff} \exp\left(-\frac{E_A}{kT_A}\right)$$

which gives,

$$t_{eff} = t \exp\left[-\frac{E_A}{k}\left(\frac{1}{T} - \frac{1}{T_A}\right)\right]$$

The right hand side of the equation can be evaluated numerically for the rise to, and fall from, the annealing temperature.

The only hitch in the above process is that the ultimate objective in making the annealing runs is to determine the activation energy. The problem can be circumvented by first calculating a trial activation energy using the uncorrected times at temperature. Then, using this trial activation energy we can calculate the effective time at temperature. The activation energy is then recalculated using the corrected annealing times.

# RESULTS

## Effect of Sample Preparation

Two sets of tests were made in order to determine whether or not the sample preparation would affect the outcome of the hardness tests. The areas of concern were the sectioning (milling) and the etching processes.

Two lengthwise hardness profiles were made on sample U-7-042-OH-2. The first profile was made on what was an original surface of the Charpy bar half while the second profile was made on the opposite (milled) surface of the sample. The two samples were ground and polished in an identical manner. Figure 7 reveals no difference between the two profiles (the difference in average weld metal hardness values is well within data scatter). Thus, it is concluded that the sectioning process has no effect on the hardness values obtained.

In figure 7 it can also be seen that the sample has been divided into 4 different microstructure regions. Three general regions exist, the base plate, HAZ, and weld metal, as discussed before. However, upon close examination the HAZ was subdivided by hardness and microstructure into two regions. Microstructure region III of the HAZ is relatively coarse grained with a high hardness value while microstructure region II of the HAZ is fine grained with a lower hardness value. It is not completely unexpected to find two different regions in the HAZ because of, among other things, differing cooling rates across the HAZ (31,39).

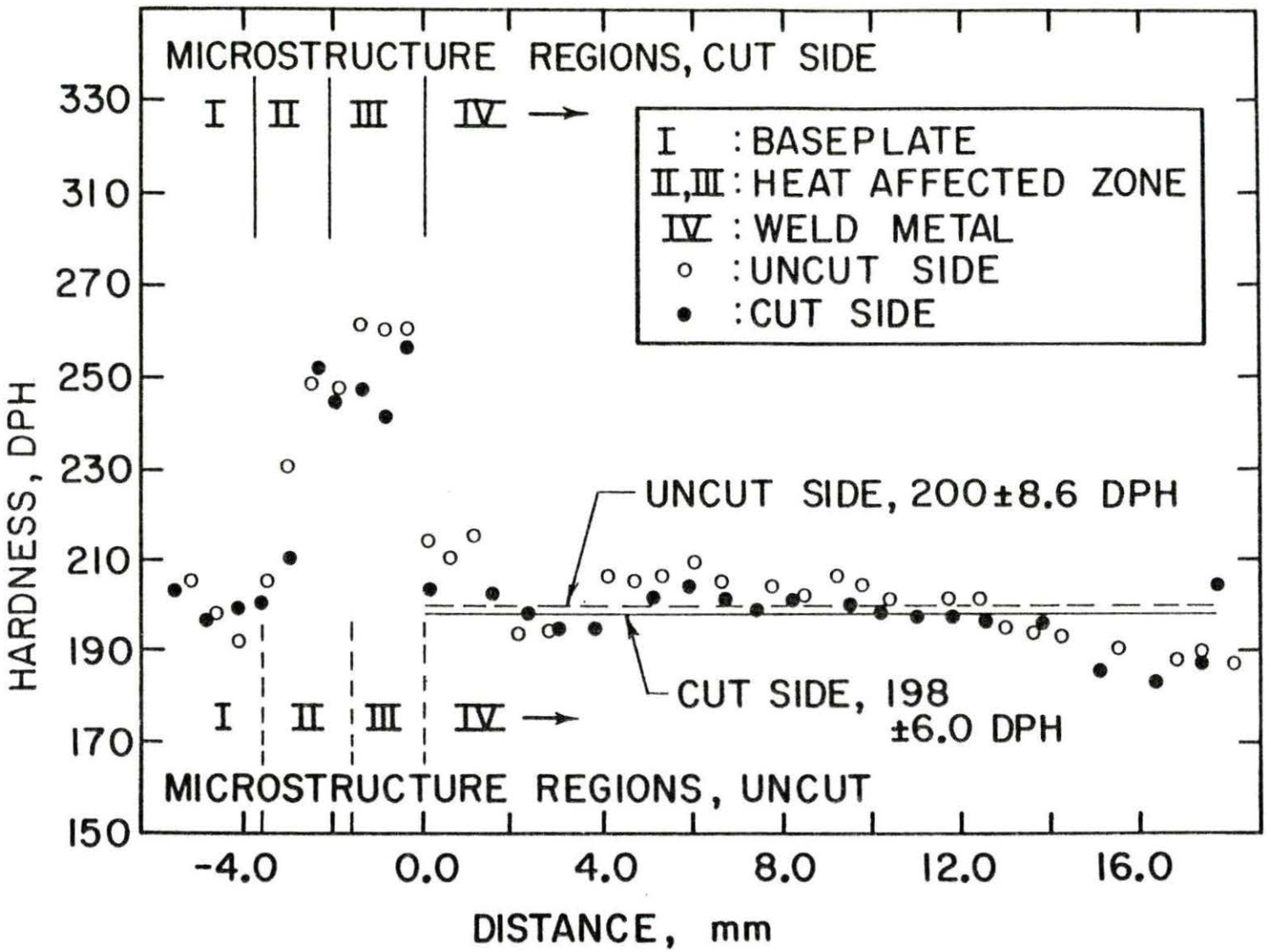


Figure 7. Comparison of hardness profiles made on opposite cut (sectioned) and uncut (original) faces of sample U-7-052-0H-2

Two series of photomicrographs were taken to show the changes in microstructure. The first series, shown in figure 8, is at low magnification (38x) and shows the general change from one region to the next. The second series of photomicrographs was also taken along the length of the sample and can be seen in figure 9. The magnification for the second series of photomicrographs is at 250X to reveal the microstructure in greater detail.

The other area of concern in the preparation process was the light etching of the metal (recall that this was done to allow the experimenter to test a specific microstructure region, e.g., weld metal, if so desired). Two hardness profiles were made on U-3-007-0H-1 in order to determine whether or not the etching had an effect on the hardness value obtained. The first hardness profile was made after the sample was polished but before etching and the second profile was made after the etching. Figure 10 shows that the etching process did not affect the hardness. Again, the difference in the average weld metal hardness is well within the data scatter.

## Effects of Irradiation

The effects of irradiation were measured by making hardness measurements on irradiated and unirradiated samples from three different heats of steel. All three heats, numbered 3, 7, and 10, show fairly significant radiation hardening, as can be seen in figures 11, 12, and 13, respectively. The fluence for each of the heats was approximately $1 \times 10^{18}$ $n/cm^2$, $E > 1MeV$.

Figure 8. Series of photomicrographs at 38X revealing the change in microstructure in going from one end of half of a Charpy bar towards the fractured surface (a) The first 4 indentations are in the base plate (b) Indentations 5 through 8 are in Region II of the HAZ (c) Indentations 9 and 10 are in Region III of the HAZ, while 11 and 12 are in the weld

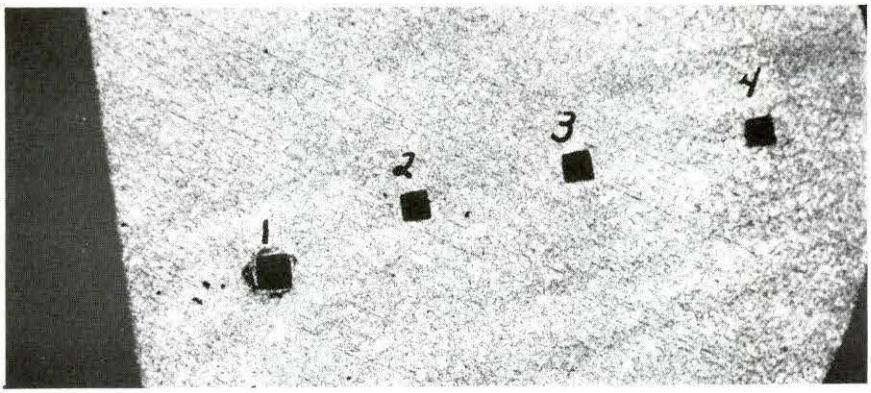


(a)

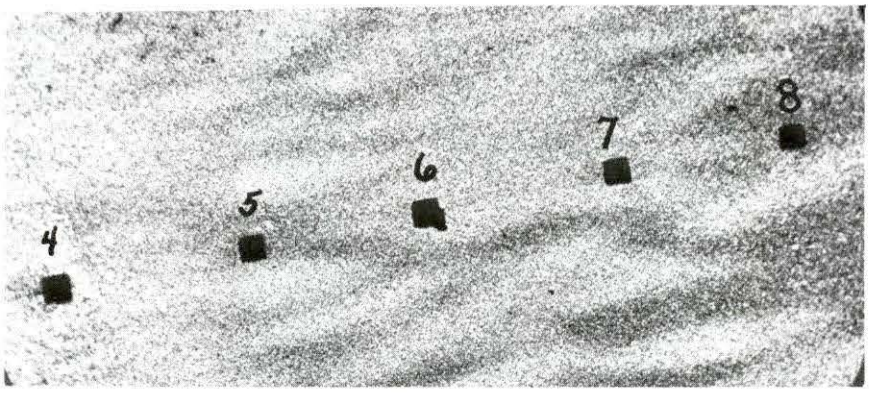


(b)

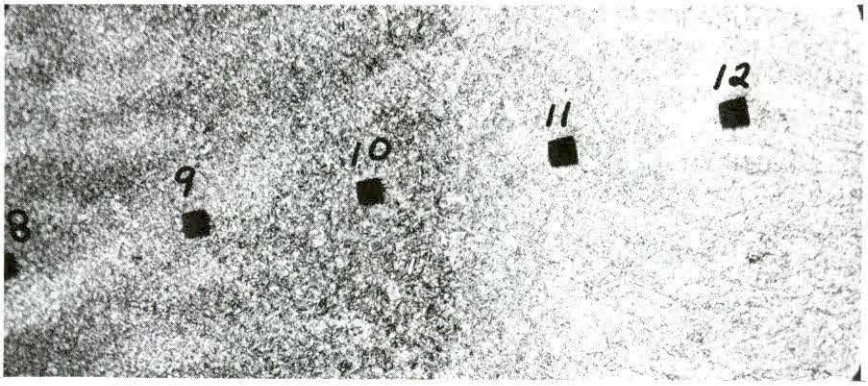


(c)

(a)

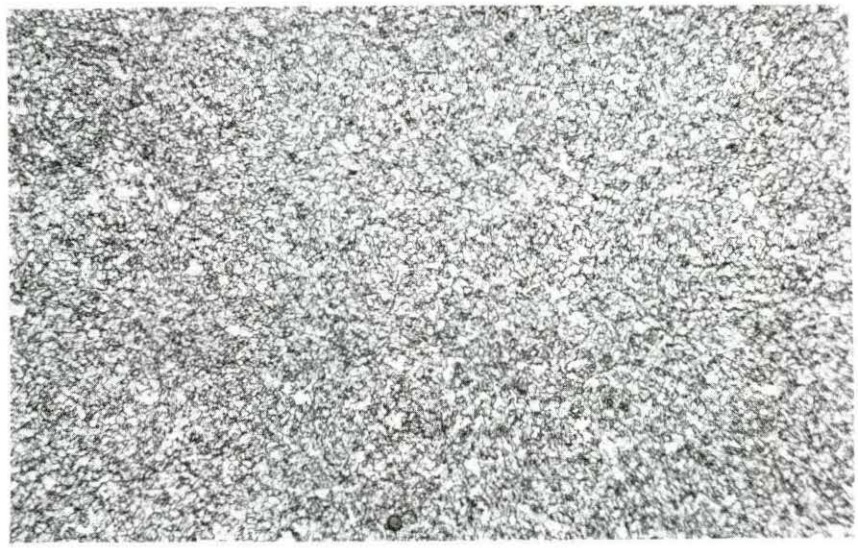

(b)

Figure 9. Series of photomicrographs at 250X revealing the detailed grain appearance exhibited by the 4 different microstructure regions in a half of a Charpy bar. (a) Base plate region at left with the beginning of the transition to the HAZ at right (b) Region II of HAZ (c) Beginning of Region III of HAZ (d) Transition from Region III to weld with weld metal at right

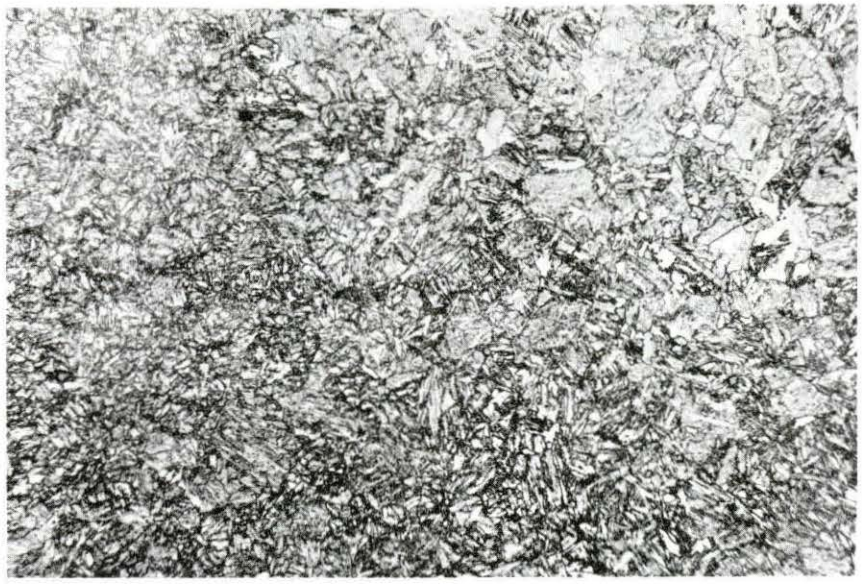

(c)

Figure 9 (continued) (d)

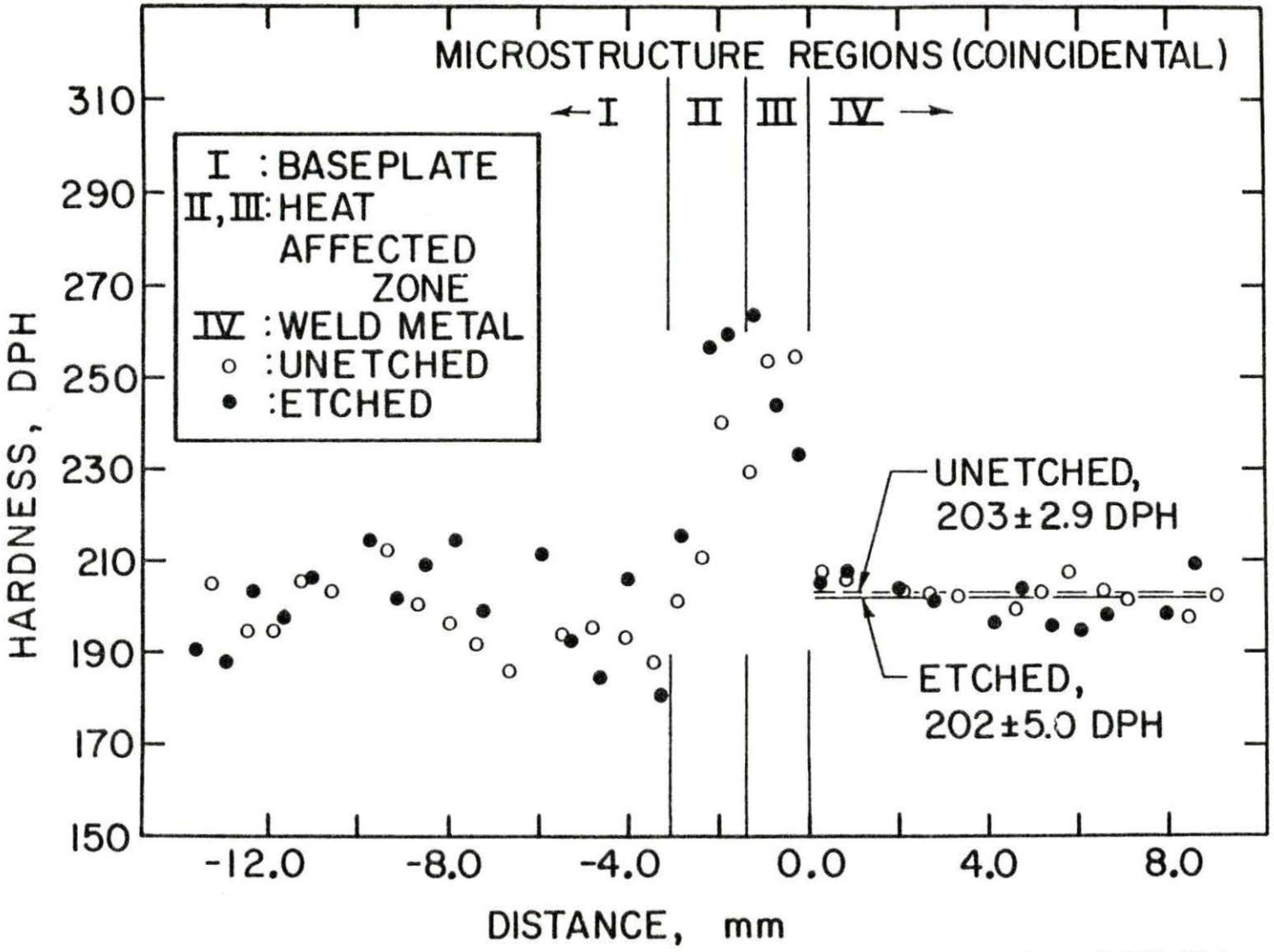


Figure 10. Comparison of unetched and etched hardness profiles for sample U-3-007-011-1

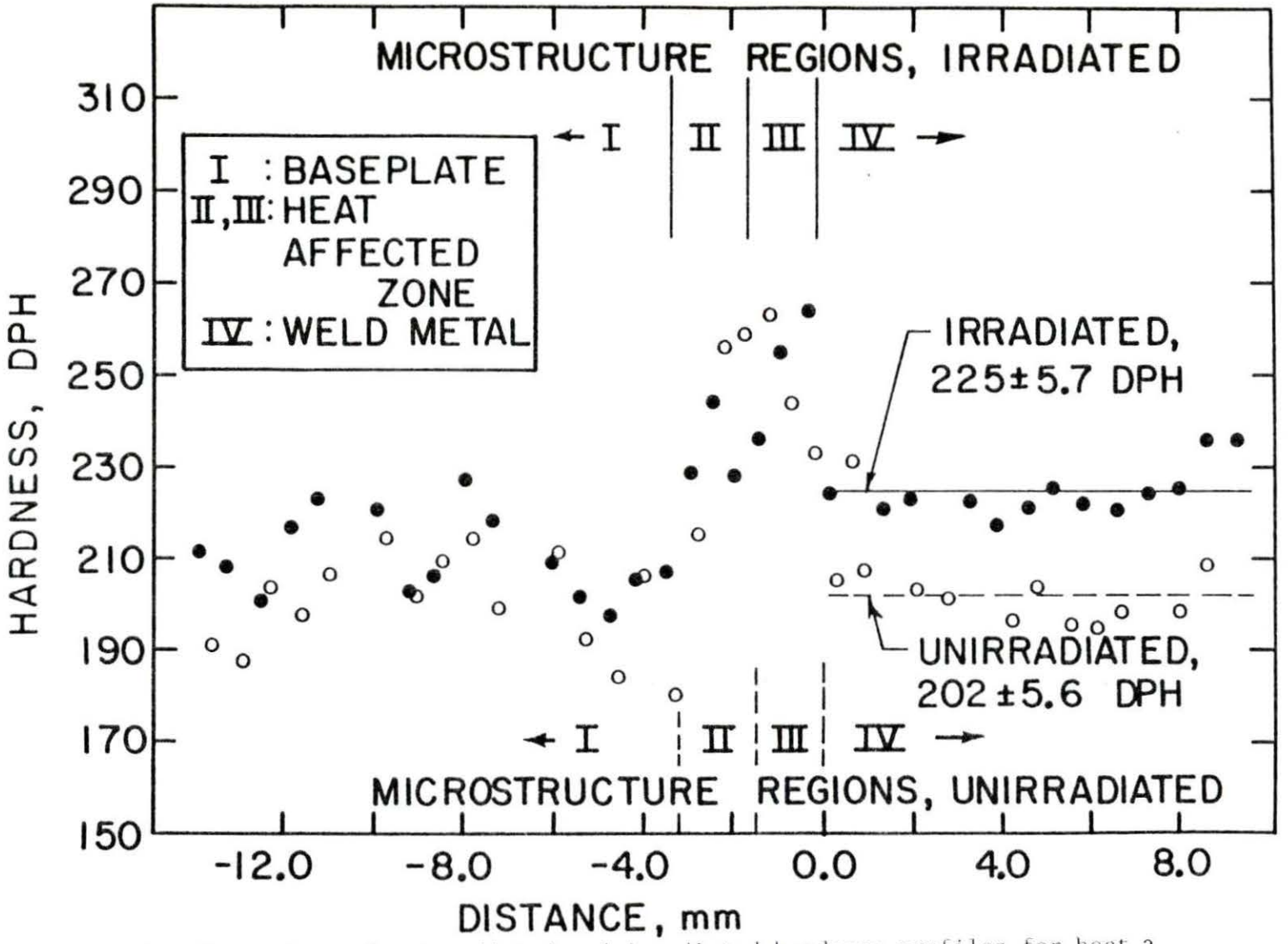


Figure 11. Comparison of unirradiated and irradiated hardness profiles for heat 3

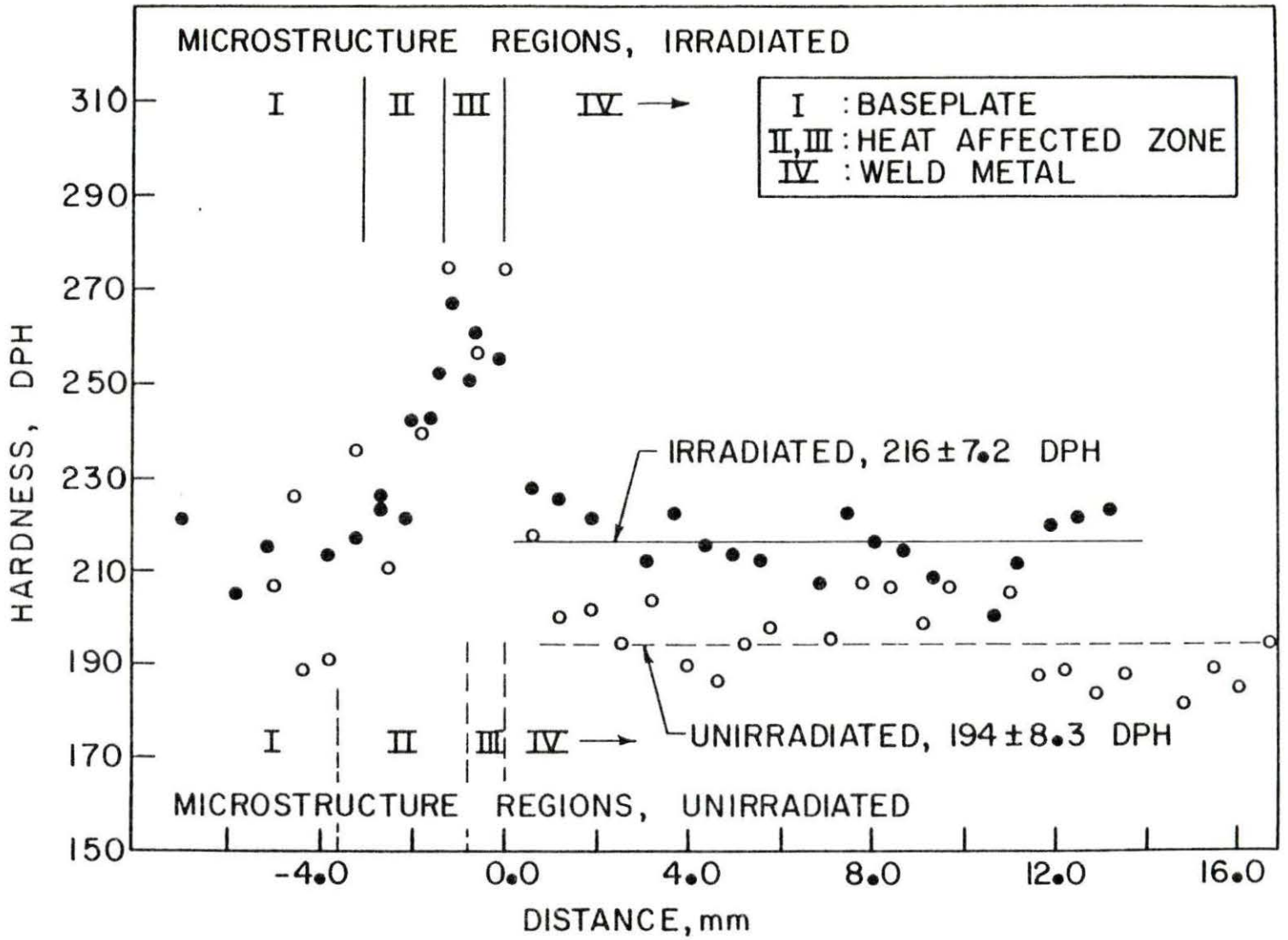


Figure 12. Comparison of unirradiated and irradiated hardness profiles for heat 7

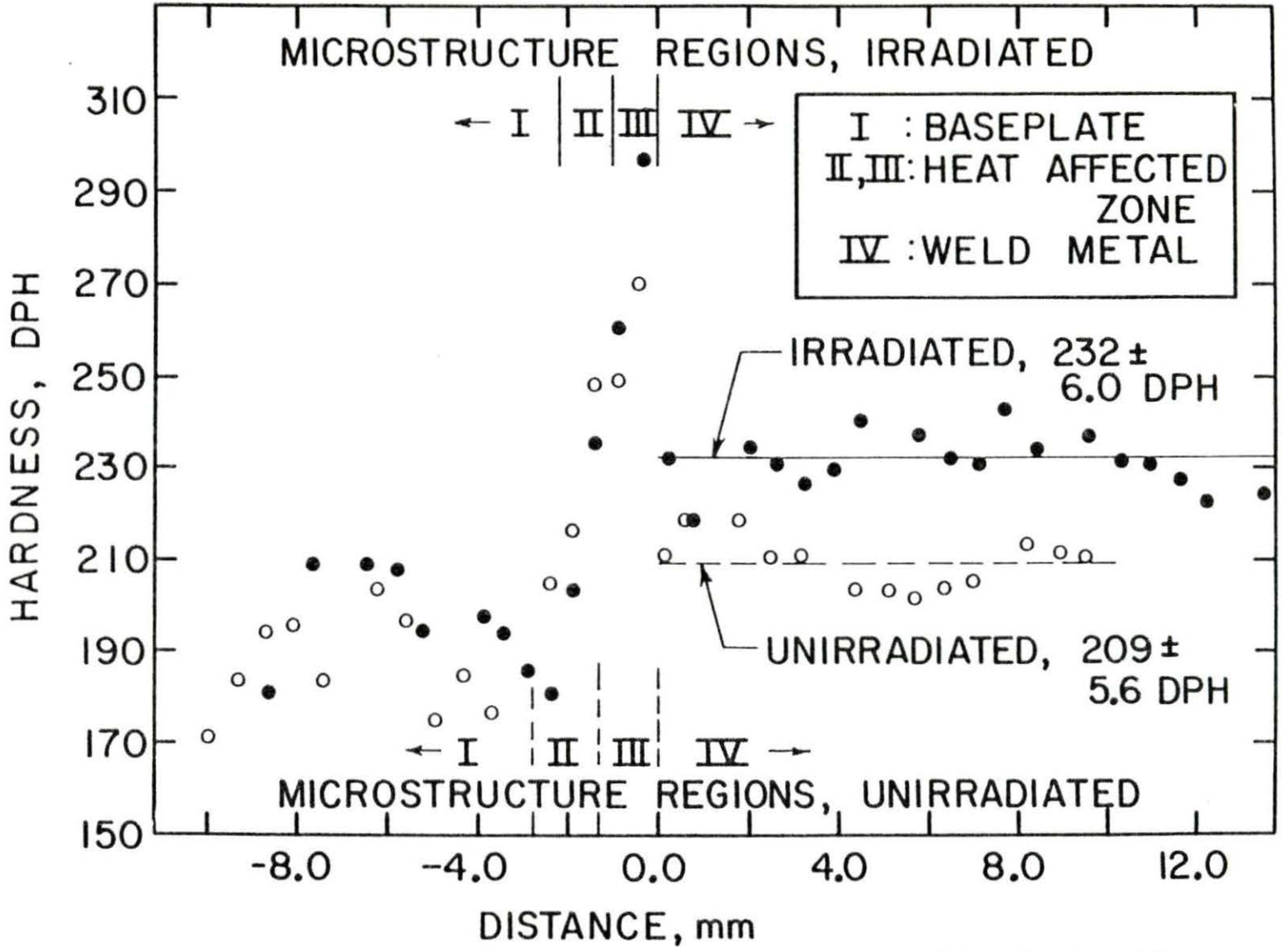


Figure 13. Comparison of unirradiated and irradiated hardness profiles for heat 10

In all cases, the weld metal shows about a 10% increase in hardness upon irradiation. The base plate shows very little increase in hardness that can be distinguished from data scatter. Heat 3 (in figure 11) shows the only notable increase in base plate hardness. The HAZ hardness does not seem to be affected at all by the irradiation.

## Recovery Data

All of the following annealing tests were done on samples from the same Charpy bar half. The isochronal annealing runs were conducted on sample I-7-007-OH-3. Two sets of isothermal annealing runs were conducted: the 415 degrees C runs on I-7-007-OH-2 and the 445 degrees C runs on I-7-007-OH-4. Unirradiated control samples (from the same heat of steel as the irradiated samples) were subjected to the same annealing conditions as the irradiated samples. This was done in order to determine if the hardness of the control samples was changed as a result of the annealing treatments. No such change was observed.

The isochronal recovery curve for sample I-7-007-OH-3 is plotted in figure 14. The isochronal annealing runs were conducted for a nominal time of 1 hour (with an actual corrected annealing time of 1 hour and 10 minutes). As can be seen in figure 14, the recovery occurs between approximately 400 and 500 degrees C.

The fractional recovery, f, used in all the recovery curves is defined as follows.

$$f = (H-H_f)/(H_i-H_f)$$

where H is the average weld metal hardness measured after each annealing

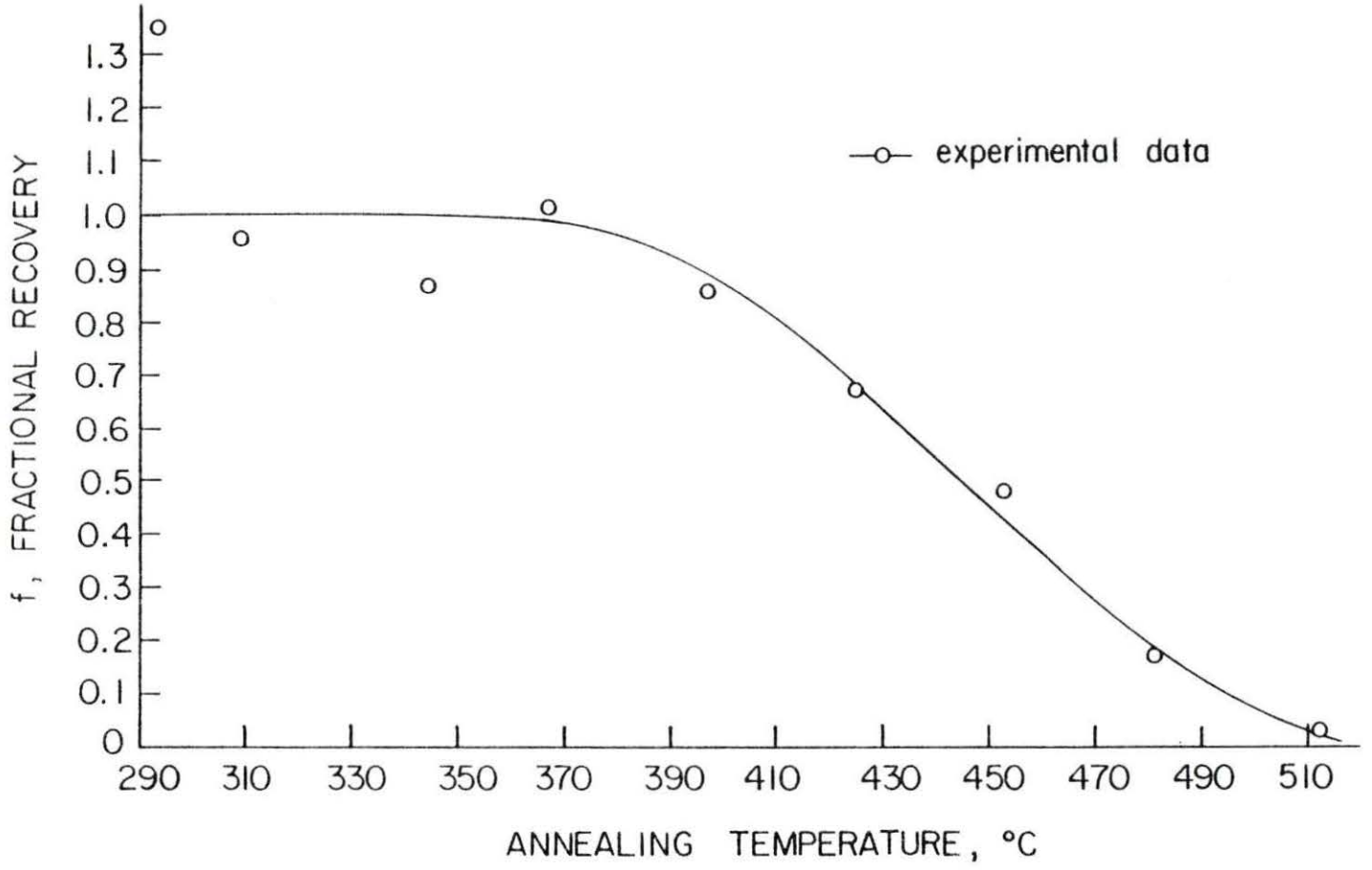


Figure 14. Isochronal recovery curve for sample I-7-007-OH-3

run, $H_i$ is the average weld metal hardness in the irradiated, unannealed state, and $H_f$ is the average weld metal hardness in the unirradiated state.

Figure 15 shows the 415 degrees C isothermal recovery of I-7-007-OH-2. Here the uncertainty posed by the data scatter was large enough so that an exponential, least squares data fit was made. There was no reason to believe that the annealing process had more than a single activation energy. Therefore, the general form of the exponential used was

$$f = e^{-bt} \tag{1}$$

which is the general form for a singly activated, first order process. t is equal to the annealing time and b is a constant.

The exponential form in Equation (1) was used instead of

$$f = c\, e^{-bt}$$

where c is a constant because it is required that f = 1.0 at t = 0. Anything other than f = 1.0 at an annealing time t = 0 would be meaningless.

It should be noted here that the annealing time plotted is the total corrected annealing time including the correction for an effective time at temperature during heatup and cooldown (see discussion in Annealing Procedure).

The 445 degrees C isothermal recovery of I-7-007-OH-4 is shown in figure 16 and the annealing time is also the total corrected time at temperature. Again an exponential, least squares data fit was used.

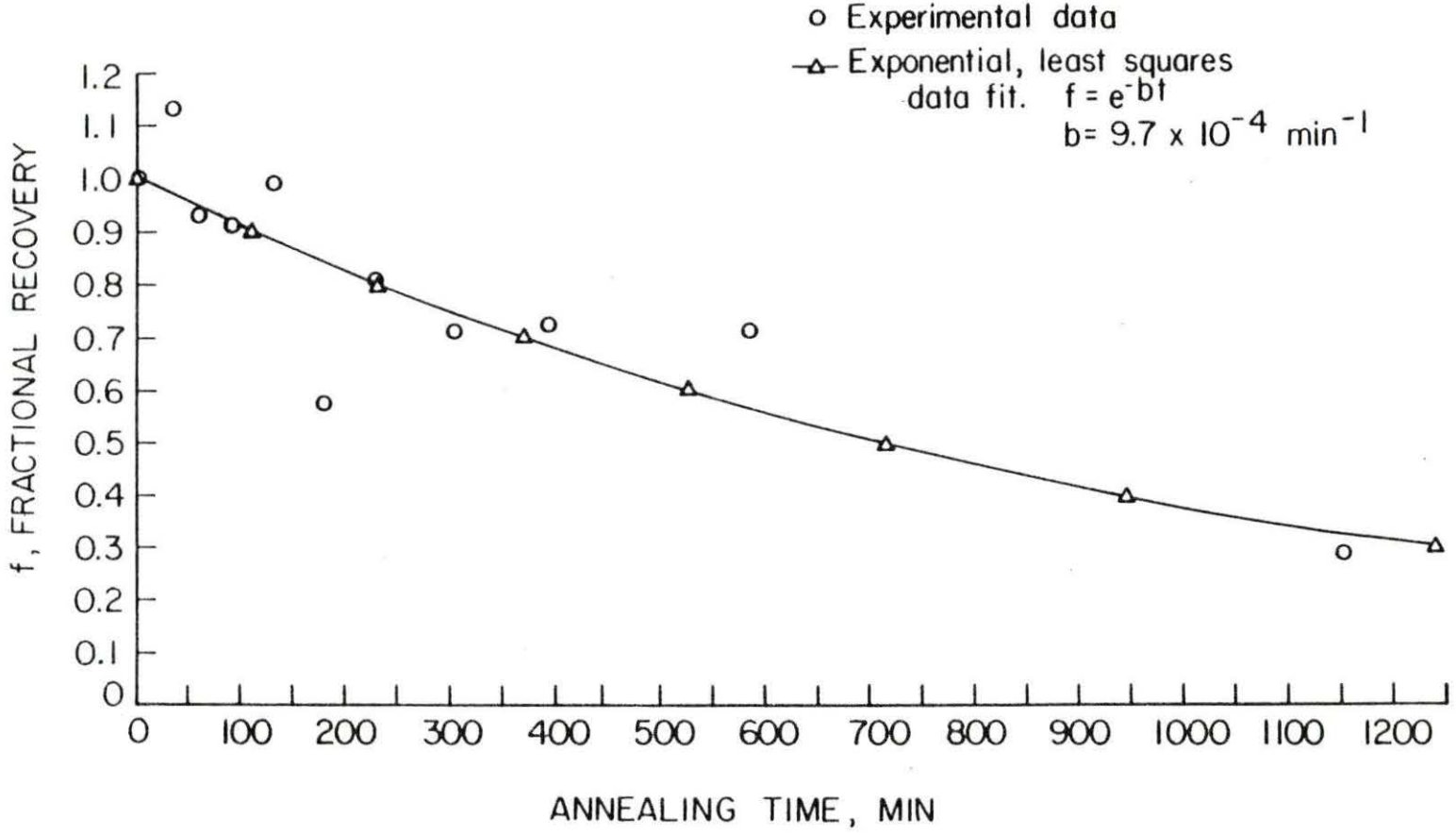


Figure 15. Isothermal (415 degrees C) recovery curve for sample I-7-007-OH-2

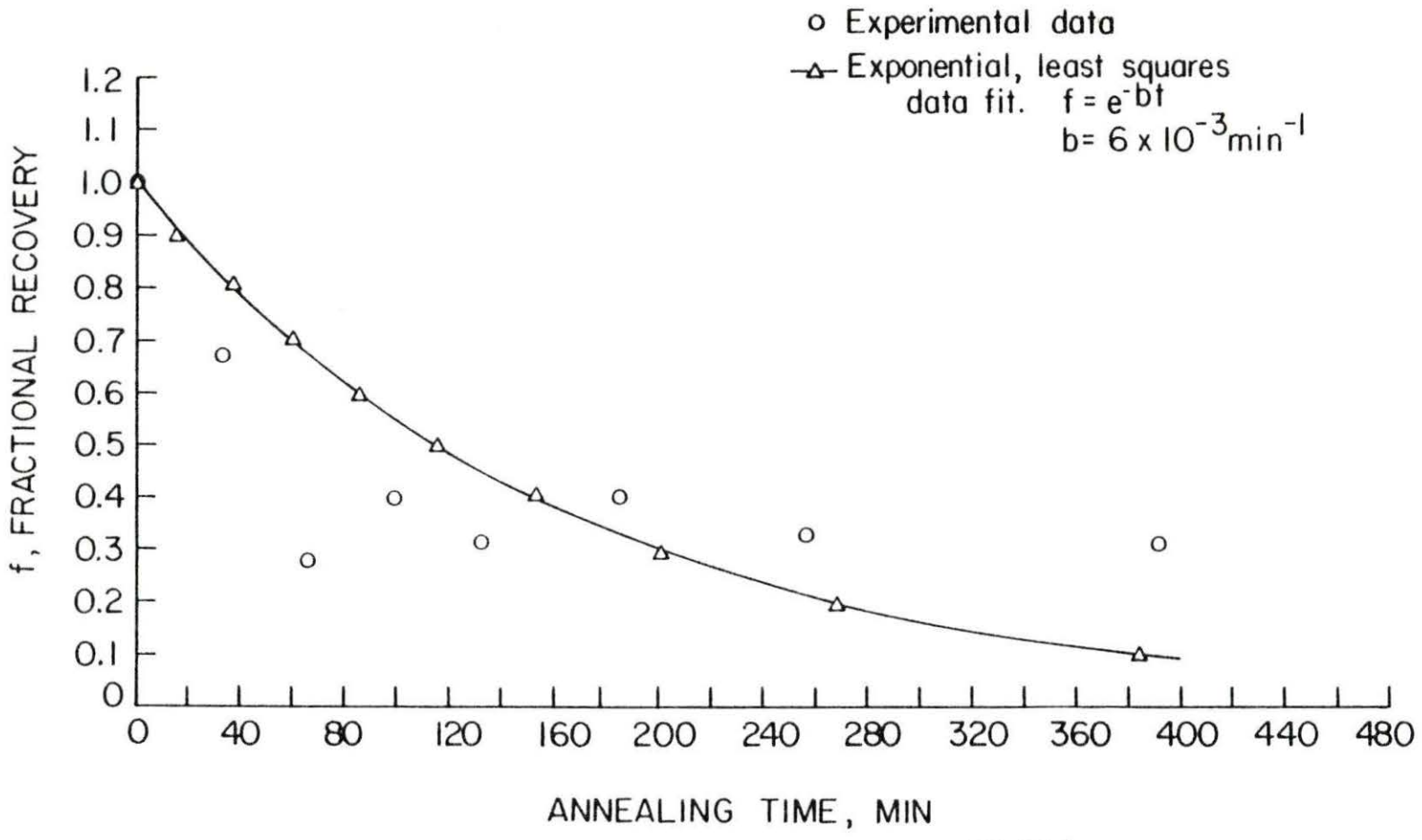


Figure 16. Isothermal (445 degrees C) recovery curve for sample I-7-007-011-4

## Activation Energy Analysis

The method for determining the activation energy is briefly described here. Let $C_d$ be the concentration of radiation-produced defect clusters, assumed here to be the hardening agents. The annealing rate is considered to be of the form

$$-\frac{dC_d}{dt} = K(T)F(C_d) \tag{2}$$

where $K(T)$ is the rate constant and $F(C_d)$ is a function whose form depends on the annihilation event. For a singly activated process we may take

$$K(T) = \nu_o \exp(-\frac{E_A}{kT}) \tag{3}$$

where $E_A$ is the (single) activation energy and $\nu_o$ is a temperature independent frequency. Equation (3) in (2) gives

$$-\frac{dC_d}{dt} = \nu_o \exp(-\frac{E_A}{kT})\ F(C_d) \tag{4}$$

Upon integration of (4), we have

$$-\int_{(C_d)_o}^{C_d} \frac{dC_d}{F(C_d)} = t\ \nu_o \exp(-\frac{E_A}{kT}) \tag{5}$$

We may assume that the fractional departure from completion of the annealing, f, is proportional to $C_d$, so that (5) may be written

$$-\int_{f=1}^{f} \frac{df}{F(f)} = t\ \nu_o \exp(-\frac{E_A}{kT}) \tag{6}$$

Then, if we let the left-hand side of (6) be given by g(f) we have

$$g(f) = t\ \nu_o\ \exp\ (-\frac{E_A}{kT}) \tag{7}$$

The Meechan-Brinkman method for determining the activation energy for the recovery process (40) uses one isothermal recovery curve and one isochronal recovery curve, as is shown schematically in figure 17. Since the isochronal anneal for time $\Delta t_b$ at temperature $T_b$ is equivalent to the isothermal anneal for time $\Delta t_a$ at temperature $T_a$, we see from Equation (7) that

$$\Delta t_a\ \exp(-\frac{E_A}{kT_a}) = \Delta t_b\ \exp(-\frac{E_A}{kT_b}) \tag{8}$$

In the Meechan-Brinkman approach, a number of isothermal time intervals, $\Delta t_a$'s, are deduced corresponding to a number of isochronal temperatures, $T_b$'s. Grouping the factors in Equation (8) accordingly, we have

$$\ln\ \Delta t_a = (\ln\ \Delta t_b + \frac{E_A}{kT_a}) - \frac{E_A}{k}\ \frac{1}{T_b}$$

where the expression in parentheses is a constant. Thus, if $\ln\ \Delta t_a$ is plotted versus $1/T_b$, a straight line of slope $(-E_A/k)$ should result.

Figure 18 shows the results of the Meechan-Brinkman analyses. The activation energy calculated is $0.60 \pm 0.06$eV. The $\Delta t_a$'s of the data points on the figure are from the least squares data fits for the isothermal recovery curves. Least squares data fits were used for the straight lines in figure 18. The activation energies and their associated errors were calculated from the least squares line.

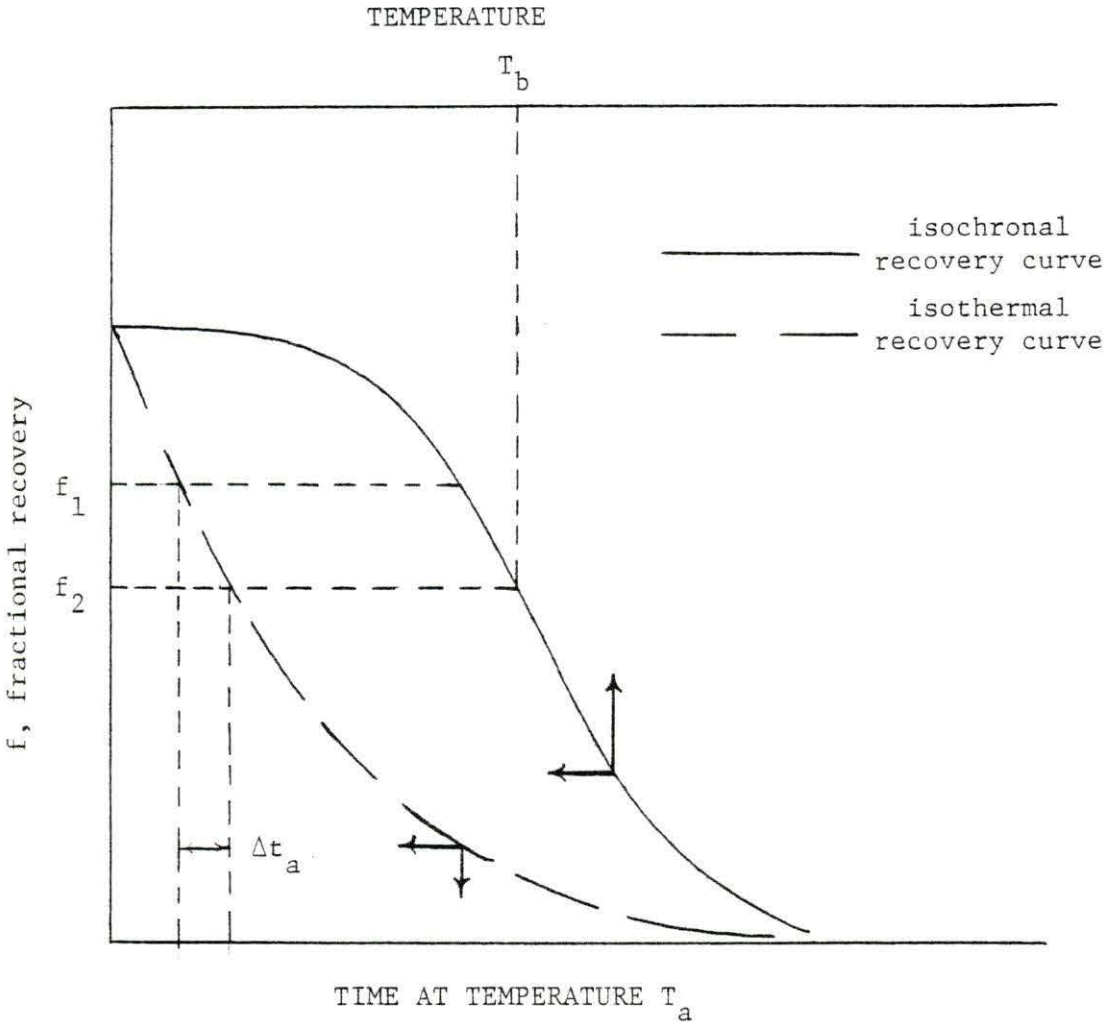


Figure 17. Schematic diagram of Meechan-Brinkman method for activation energy analysis

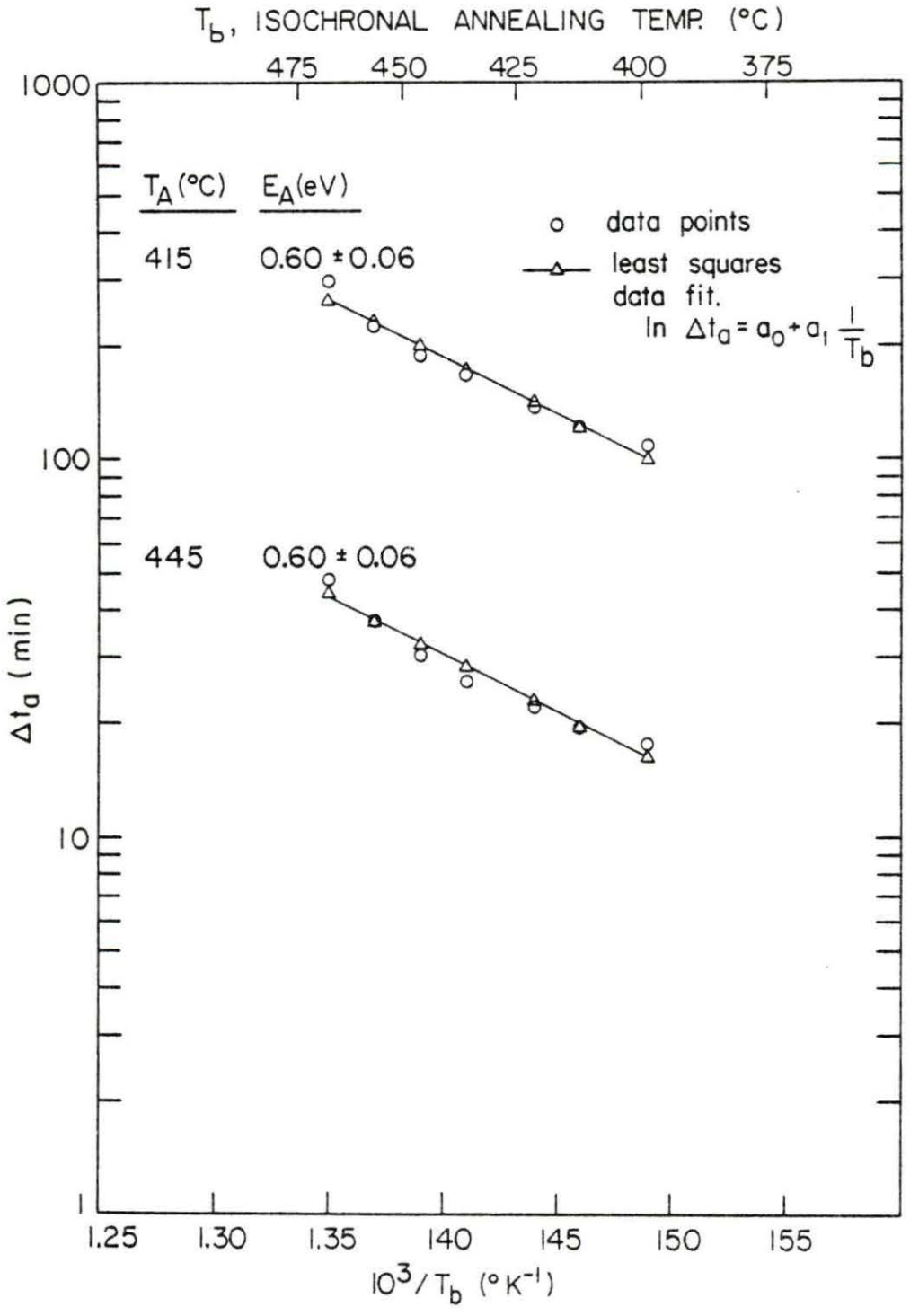


Figure 18. Results of Meechan-Brinkman energy analysis for heat 7

# DISCUSSION

The microstructure of the bars was similar to what was expected, except for the need to subdivide the HAZ into two separate regions. According to the Metals Handbook (31) the presence of more than one microstructure region in an HAZ is not surprising. In a hardenable carbon steel, the base metal immediately adjacent to the weld metal may be coarse grained because a temperature in the range of 2200 to 2800 degrees F has been reached. A temperature that high allows new grains to nucleate and grow. Further away from the weld the HAZ is expected to have a finer grain structure because even though it too was raised above the transformation temperature, the time at temperature was not sufficient to cause grain coarsening.

Considering only the Hall-Petch equation (discussed in the Radiation Hardening section) the finer grained portion of the HAZ should have a higher hardness value than the coarse grained region. Just the opposite was found to be the case, though. With a little thought, the situation is not really anomalous because the Hall-Petch equations does not necessarily hold when comparing two different phases, e.g., bainite and pearlite. It is possible to find several different phases in the HAZ (39) and, thus, it is entirely acceptable for the coarser grained region to have a higher hardness than the finer grained region.

The radiation response of the three heats of steel was just as might be expected. The weld metal showed greater radiation sensitivity than the base plate or the HAZ. This is in agreement with the fact

that weld metals are, in general, the life limiting metal of the reactor pressure vessel.

Further, a radiation-produced hardness increase of 10% at a fluence of $1 \times 10^{18}$ n/cm$^2$, E > 1MeV, is quite reasonable. Spitznagel et al. (28) reported an increase in hardness of approximately 20% for weld metal subjected to a neutron fluence of $5.7 \times 10^{18}$ n/cm$^2$, E > 1MeV. Pachur (41) shows an increase of between 5 and 13% for A533 B steel irradiated to a fluence of $1 \times 10^{19}$ n/cm$^2$, E > 1MeV. Although there is obviously a variation in radiation response, the results agree in general.

The isochronal recovery curve is in good agreement with work done by Pachur (41). The two sets of results cannot be directly compared in terms of fractional recovery because the A302 B steel in Pachur's study was irradiated to a much higher fluence ($1 \times 10^{20}$ n/cm$^2$, E > 1MeV). However, it is interesting to note that full recovery occurs between approximately 400 and 500 degrees C in both cases.

The isothermal recovery curves compare favorably with work done by Spitznagel et al. (28). Spitznagel investigated the 427 degrees C isothermal recovery of a weld metal irradiated to a fluence of $5.7 \times 10^{18}$ n/cm$^2$, E>1MeV. Spitznagel's work showed f = 0.75 at t = 60 minutes and f = 0.53 at t = 1080 minutes. This compares to the 415 degrees C results of f = 0.93 at t = 60 min. and f = 0.35 at t = 1080 min. The 445 degrees C results show that at t = 60 min., f = 0.70 while no comparison can be made at the longer time because the recovery process is completed by that time. The times of 60 min. and 1080 min. were chosen because they corresponded to actual data of Spitznagel.

The value of f = 0.75 obtained by Spitznagel after 60 min at 427 degrees C is roughly consistent with the values of f = 0.93 and 0.70 obtained in the present work after 60 min at 415 and 445 degrees C, respectively. In general, in view of the data scatter present in hardness testing, the results reported here are in agreement with the results of earlier work.

The activation energy analysis is interesting because it gives some clues as to what is occurring during the recovery process and, ultimately, to the nature of the radiation-produced defect clusters themselves. The activation energy calculated, 0.60 eV, is approximately equal to the migration energy for monovacancies in alpha iron, 0.68 eV (42). The 0.68 eV is characteristic of vacancy migration along <111> directions in alpha iron.

From the above, it could be surmised that the radiation-produced defects are vacancy clusters or small voids that anneal away by emitting single vacancies.

An alternative explanation would be that the defect clusters are divacancies or trivacancies. The migration energy for, both, divacancies and trivacancies is 0.66 eV (42). Also, from field ion microscope observations by Spitznagel, the vacancy clusters should be approximately 7 to 10 $\mathring{A}$ in size. This nearly agrees with the estimated size of trivacancies 5.7 $\mathring{A}$, while the sizes of divacancies, quadvacancies, and quintvacancies are estimated to be 2.9, 8.6 and 11.5 $\mathring{A}$, respectively (42). Thus, with close agreement between the estimated size and the migration energy the defect clusters

could be trivacancies which migrate as a whole to annihilation at a sink. Migration of entire defect clusters is also suggested by Nichols (8). The actual size and nature of the clusters cannot be determined by annealing studies, but it seems clear that they could be vacancy in nature.

## SUMMARY

This investigation can be summarized by the following conclusions:

1. The three heats of pressure vessel steel all showed, approximately, a 10% increase in the average weld metal hardness when irradiated to a fluence of about $1 \times 10^{18}$ $n/cm^2$, $E > 1$ MeV. The base plate also showed a general increase in hardness. There was no noticeable increase in the hardness of the heat affected zone.
2. The activation energy, as determined by the Meechan-Brinkman method, for the recovery of radiation induced hardness was found to be $0.60 \pm 0.06$ eV.
3. The activation energy of 0.6 eV is approximately equal to that calculated for vacancy migration in alpha iron, suggesting that the radiation-produced defect clusters are vacancy in nature.

# BIBLIOGRAPHY


1. Standard Specification for Pressure Vessel Plates, Alloy Steel, Manganese-Molybdenum and Manganese-Molybdenum-Nickel, ASTM A302-78, in Annual Book of ASTM Standards (American Society for Testing and Materials, Philadelphia, Pa., 1979), Vol. 4, p. 258.

2. Standard Specification for Pressure Vessel Plates, Alloy Steel, Quenched and Tempered, Manganese-Molybdenum and Manganese-Molybdenum-Nickel, ASTM A533-78, in Annual Book of ASTM Standards (American Society for Testing and Materials, Philadelphia, Pa., 1979), Vol. 4, p. 480.

3. Alfred K. Seeger, On the Theory of Radiation Damage and Radiation Hardening, in Proceedings of the Second U.N. International Conference on the Peaceful Uses of Atomic Energy (United Nations Publication, Great Britain, 1958), Vol. 6, p. 250.

4. Donald R. Olander, Fundamental Aspects of Nuclear Reactor Fuel Elements (ERDA Technical Information Center, Oak Ridge, Tennessee, 1976).

5. M. J. Makin and F. J. Minter, Irradiation Hardening in Copper and Nickel, Acta Metallurgica, 8, 691 (1960).

6. George E. Dieter, Mechanical Metallurgy (McGraw-Hill Book Company, United States, 1976), Second edition.

7. R. P. Tucker and M. S. Wechsler, Radiation Hardening in Niobium-Dependence of the Yield Stress on Neutron Dose, in Irradiation Effects (Gordon and Breach, Science Publishers Ltd., Glasgow, Scotland, 1970), Vol. 3, p. 73

8. F. A. Nichols, Theory of Radiation Embrittlement and Recovery of Radiation Damage in Ferritic Steels, Philosophical Magazine, Series 8, 14, 335 (1966).

9. M. S. Wechsler, Radiation Embrittlement in Metals and Alloys, CONF-751006-P2, in Fundamental Aspects of Radiation Damage in Metals (ERDA, Washington, D.C., 1976), p. 991.

10. R. P. Tucker, S. M. Ohr, and M. S. Wechsler, Radiation Hardening and Transmission Electron Microscopy in Niobium, in Radiation Damage in Reactor Materials (International Atomic Energy Administration, Vienna, Austria, 1969), Vol. I, p. 215.

11. R. A. Wullaert, D. R. Ireland, and A. S. Tetelman, Radiation Effects on the Metallurgical Fracture Parameters and Fracture Toughness of Pressure Vessel Steels, in Irradiation Effects on Structural Alloys for Nuclear Reactor Applications, ASTM Special Technical Publication 484 (American Society for Testing and Materials, Philadelphia, Pa., 1970), p. 20.

12. A. R. Rosenfield, E. Votava, and G. T. Hahn, Dislocations and Ductile-Brittle Transition, in Ductility (American Society for Metals, Metals Park, Ohio, 1968), p. 63.

13. M. S. Wechsler, R. G. Berggren, N. E. Hinkle and W. J. Stelzman, Radiation Hardening and Embrittlement in a Reactor Pressure Vessel Steel, in Irradiation Effects in Structural Alloys for Thermal and Fast Reactors, ASTM Special Technical Publication 457 (American Society for Testing and Materials, Philadelphia, Pa., 1969), p. 242.

14. L. P. Trudeau, Radiation Effects on Toughness of Ferritic Steels for Reactor Vessels (Rowman and Littlefield, Inc., New York, 1964).

15. Standard Recommended Practice for Effects of High-Energy Radiation on the Mechanical Properties of Metallic Materials, ASTM E184-62, in Annual Book of ASTM Standards (American Society for Testing and Materials, Philadelphia, Pa., 1977), Vol. 10, p. 343.

16. Appendix G-Fracture Toughness Requirements, in Code of Federal Regulations (U.S. Government Printing Office, Washington, D.C., 1978), Title 10, Chapter 1, p. 367.

17. Appendix H-Reactor Vessel Material Surveillance Program Requirements, in Code of Federal Regulations (U.S. Government Printing Office, Washington, D.C., 1978), Title 10, Chapter 1, p. 370.

18. Rules for the Construction of Nuclear Power Plant Components, in ASME Boiler and Pressure Vessel Code (American Society of Mechanical Engineers, New York, 1974), Section III, Subsection NB, p. 13.

19. Standard Recommended Guide for In Service Annealing of Water Cooled Nuclear Reactor Vessels, ASTM E509-74, in Annual Book of ASTM Standards (American Society for Testing and Materials, Philadelphia, Pa., 1977), Vol. 45, p. 980.

20. Appendix G-Protection Against Nonductile Failure, in ASME Boiler and Pressure Vessel Code (American Society of Mechanical Engineers, New York, 1974), Section III, Subsection NA, p. 487.

21. L. E. Steele, P. N. Randall, K. E. Stahlkopf, and S. E. Yanichko, Reactor Vessel Surveillance, in Nuclear Engineering Materials Handbook (to be published), Vol. I, Chapter 2.

22. N. H. Polakowski and E. J. Ripling, Strength and Structure of Engineering Materials (Prentice-Hall, Inc., Englewood Cliffs, New Jersey, 1966).

23. M. S. Wechsler, The Influence of Impurity-Defect Interactions on Radiation Hardening and Embrittlement, Journal of Engineering Materials and Technology, 101, 114 (1979).

24. F. A. Smidt and L. E. Steele, Residual Elements and Irradiation Embrittlement, NRL Report 7310 (Naval Research Laboratory, Washington, D.C., 1971).

25. R. A. Wullaert, J. W. Sheckherd, and R. W. Smith, Evaluation of the Maine Yankee Reactor Beltline Materials, in Irradiation Effects on the Microstructure and Properties of Metals, ASTM Special Technical Publication 611 (American Society for Testing and Materials, Philadelphia, Pa., 1976), p. 400.

26. Effects of Residual Elements on Predicted Radiation Damage to Reactor Vessel Materials, Regulatory Guide 1.99 (U.S. Nuclear Regulatory Commission, Washington, D.C., 1977), Revision 1.

27. M. S. Wechsler, Impurity-Defect Interactions and Radiation Hardening in BCC Metals, in Proceedings, Discussion Meeting on Defects in Refractory Metals, edited by R. Debatist, J. Nihoul, and L. Stals (SCK-CEN, Mol, Belgium, 1972), p. 235.

28. J. A. Spitznagel, R. P. Shogan, and J. H. Phillips, Annealing of Irradiation Damage in High-Copper Ferritic Steels, in Irradiation Effects on the Microstructure and Properties of Metals, ASTM Special Technical Publication 611 (American Society for Testing and Materials, Philadelphia, Pa., 1976), p. 434.

29. J. R. Hawthorne, H. E. Watson, and F. J. Loss, Exploratory Investigations of Cyclic Irradiation and Annealing Effects on Notch Ductility of A533 B Weld Deposits in Irradiation Effects on the Microstructure and Properties of Metals, ASTM Special Technical Publication 683, edited by J. A. Sprague and D. Kramer (American Society for Testing and Materials, Philadelphia, Pa., 1978), p. 278.

30. J. R. Hawthorne, Survey of Postirradiation Heat Treatment as a Means to Mitigate Radiation Embrittlement of Reactor Vessel Steels, NRL Report 8287 (Naval Research Laboratory, Washington, D.C., 1979).

31. Submerged-Arc Welding, in Metals Handbook (American Society for Metals, Metals Park, Ohio, 1970), Eigth Edition, Vol. 6, p. 46.

32. J. R. Hawthorne, J. J. Koziol, and R. C. Groeschel, Evaluation of Commercial Production A533 B Plates and Weld Deposits for Improved Radiation Embrittlement Resistance, in Properties of Reactor Structural Alloys After Neutron or Particle Irradiation, ASTM Special Technical Publication 570 (American Society for Testing and Materials, Philadelphia, Pa., 1975), p. 83.

33. J. R. Hawthorne, J. J. Koziol, and S. T. Byrne, Evaluation of Commercial Production A533 B Steel Plates and Weld Deposits with Extra-Low Copper Content for Radiation Resistance, in Irradiation Effects on the Microstructure and Properties of Metals, ASTM Special Technical Publication 683 (American Society for Testing and Materials, Philadelphia, Pa., 1978), p. 235.

34. J. R. Hawthorne, Demonstration of Improved Radiation Embrittlement Resistance of A533 B Steel Through Control of Selected Residual Elements, NRL Report 7121 (Naval Research Laboratory, Washington, D.C., 1970).

35. J. R. Hawthorne, Further Observations on A533 B Steel Plate Tailored for Improved Radiation Embrittlement Resistance, NRL Report 7917 (Naval Research Laboratory, Washington, D.C., 1975).

36. Standard Method of Test For Vickers Hardness of Metallic Materials, ASTM E92-72, in Annual Book of ASTM Standards (American Society for Testing and Materials, Philadelphia, Pa., 1975), Vol. 10, p. 209.

37. Drawings for Micro Hot-Hardness Tester, Drawings D-5006-1 through D-5006-8, Oak Ridge National Laboratory, Oak Ridge, Tennessee.

38. E. Borje Bergsman, Some Recent Observations in Micro-Hardness Testing, ASTM Bulletin, 176, 37 (1951).

39. A. S. Tetelman and A. J. McEvily, Jr., Fracture of Structural Materials (John Wiley and Sons, Inc., New York, 1967).

40. C. J. Meechan and J. A. Brinkman, Electrical Resistivity Study of Lattice Defects Introduced in Copper by 1.25-MeV Electron Irradiation at 80 degrees K, Physical Review, 103, 1193 (1956).

41. D. Pachur, Embrittlement Saturation of Reactor Pressure Vessel Steels, Nuclear Research Center, Julich, Federal Republic of Germany (unpublished).

42. J. R. Beeler, Jr., Computer Simulation of Radiation-Induced Void Nucleation and Growth in Metals, in Radiation-Induced Voids in Metals, edited by J. W. Corbett and L. C. Ianniello (National Technical Information Service, Oak Ridge, Tennessee, 1972), p. 684.

ACKNOWLEDGMENTS

I would like to thank Dr. Monroe S. Wechsler for his suggestions on this thesis and for the willing manner in which he gave them. Thanks also go to Wes Alexander for his help in the construction of the experimental apparatus for the project and to Jo Sedore for typing the thesis. I also appreciate the support and cooperation of Dr. T. U. Marston and the Electric Power Research Institute, Palo Alto, California, and Mr. A. L. Lowe, Jr., and the Babcock and Wilcox Company, Lynchburg, Virginia. Finally, I am grateful to the technical staff at Ames Laboratory and to Mr. R. S. Crouse of the Oak Ridge National Laboratory for assistance in various phases of the work.